IMPERIAL COLLEGE LONDON

Faculty of Engineering

Department of Civil and Environmental Engineering

The Development of Osteoarthritis as a Consequence of Bone and Cartilage Degradation

Stewart Harris McLennan

2016-2017

DECLARATION OF OWN WORK

Declaration:

This submission is my own work. Any quotation from, or description of, the work of others is acknowledged herein by reference to the sources, whether published or unpublished.

Signature : _____

Abstract

Osteoarthritis (OA) is known to affect both the bone and soft tissue of the knee joint. To effectively model degradation of the joint under the effects of OA, consideration of both the changes in the bone and soft tissue must be made. Previous efforts to do this using microscale models carried high computational demand while less computationally demanding macroscale models suffered a lack of accuracy. A balance can be struck between the two modelling scales by using mesoscale models.

The soft tissue components of the joint, the cartilage and menisci, are best represented using biphasic and depth-dependent properties. This is best done using microscale modelling. As such, this dissertation aimed to combine mesoscale bone parts with microscale soft tissue parts into a single finite element (FE) model to produce both realistic and computationally inexpensive results. This is termed a multiscale model.

To further increase the models capacity, a bone adaption algorithm was implemented to simulate the mechanostat nature of bone, in other words, the ability of bone to reabsorb and grow in certain locations in response to different loading patterns. After the initial modelling process, validation of the full three-dimensional (3D) model was made using the following loading scenarios; bodyweight loading for both healthy and damaged knee joints, knee joint misalignment as observed in patients with advanced OA and finally, level-walking gait cycle analysis.

The multiscale model was found to compare well with previous studies when investigating stress distribution and pore pressure response of the femur and femoral cartilage, respectively. Also, the model proved more computationally efficient in comparison to macroscale-only studies while maintaining an accepted level of correlation with the findings of microscale-only studies.

The obtained findings of this dissertation, specifically those when analysing the healthy versus damaged models, will hopefully influence the clinical treatment of patients suffering from all levels of OA severity.

Keywords: osteoarthritis; bone adaption; degradation modelling; microscale; mesoscale; multiscale; finite element; bodyweight loading; joint misalignment; gait cycle; biomechanics.

Acknowledgements

My deepest graduate to Dr Andrew T. M. Phillips who has guided me through this dissertation while helping me further my knowledge in the field of biomechanics.

Thanks to Mr Dan Zaharie who was always more than willing to offer me his valuable time to help throughout the software modelling aspects of the dissertation.

I extend my gratitude to all the faculty at the Royal British Legion Centre for Blast Injury Studies at Imperial College. Without their research into the foundations of this project, I would not have brought it to where it is today.

Finally, I thank my family whose support extends far beyond the time I've spent working on this dissertation.

Contents

List of Figures

11

List of Tables

Notation

E Young's modulus

e Current void ratio

e_0 Initial void ratio

I Unit tensor

k Permeability

k_0 Initial permeability

M Constant

p Pore fluid pressure

φ_f Volume fraction of the fluid

φ_s Volume fraction of the solid

σ_E Effective solid stress

σ_f Fluid stress

σ_s Solid stress

σ_t Total stress

v Poisson's ratio

CHAPTER 1 INTRODUCTION

1.1 Degradation Modelling and Osteoarthritis

Findings have shown that OA is the leading cause of disability in the elderly (Cooper et al., 2013) while the cost of the disease on the UK economy is estimated at £12 billion annually (Mathers & Loncar, 2006). The purpose of conducting this dissertation was to analyse the effectiveness of a combined mesoscale-microscale model of the human knee joint to be used in clinical application. Using FE software, the bone parts were modelled as mesoscale while the soft tissue parts, that is the cartilage and menisci, were modelled as microscale.

In vivo testing is often too time consuming and invasive to perform, hence, computational modelling provides the framework for practical investigation. Using modern FE software, one can simulate a variety of loading scenarios on the knee joint more efficiently than would be possible when using a physical sample. From this, it is hoped the study will aid clinical application and research surrounding knee joint degradation.

The field of biomechanics was born in the seventeenth century when Galileo Galilei applied his scaling law to the bone structure study of different animals. The field was established as a branch of science that applied physics to medicine (Maquet, 1992). In the nineteenth century, Bourgery (1832) made the first detailed observations of structural architecture in trabecular bone (Roesler, 1987).

From the studying the past and present literature, a gap between the clinical research and the engineering research was identified. While the clinical literature focuses on the structural architecture of the knee joint components, the engineering literature makes use of continuum mechanics to investigate the biomechanics of the knee joint (Phillips, Villette & Modenese, 2015). The present study intended to mitigate this gap by producing a more comprehensive model with the intent of aiding clinical application.

1.2 Research Aims and Objectives

The main aim of the study was to produce a representative model of the knee joint using mesoscale bone parts and microscale soft tissue parts, both of which being characteristic of the *in vivo* conditions and computationally efficient.

The secondary aim was to use the model to better understand the link between bone and soft tissue degradation in the initiation of OA damage.

The following were the main objectives of the dissertation outlined at the start:

- To create an FE simplified, axisymmetric-geometry model of the knee joint using cylindrical. The model was to then be compared against a 3D geometry model with the objective of assessing its realism.
- To locate the regions of both the bone and soft tissue parts that undergo the greatest stress and strain under bodyweight loading. From here, conclusions could be drawn about the pathways of joint damage.
- To highlight the different mechanical responses between different mechanical components of the knee joint, those being the femur, tibia, femoral cartilage, tibial cartilage and menisci.
- To propose the appropriate clinical application of both the simplified and 3D FE models along with future suggestions for improving their utility.

1.3 Thesis Outline

The initial stage of the dissertation was to conduct a literature review of the existing studies and relevant clinical data. This is presented in Chapter 2. This included establishing the chronological development of computational knee joint models along with the generalised modelling of OA damage in individual mechanical components of the knee joint. In-depth investigation of the biomechanics of each component was carried out with the goal of incorporating these findings into the final model. This is presented in section 2.2.

In Chapter 3, simplified geometry modelling of the knee joint has been examined. The purpose of doing this was two-fold; firstly, the simplified geometry of the model enabled depth-dependent properties to be applied, which proves difficult to do when using complex 3D geometries. This included varying the Young's moduli values to simulate changes in proteoglycan (PG) content through the depth, and adding FE spring elements to model collagen fibril changes, also through the depth. Secondly, the simplification of geometry allows for improved computational efficiency. From here, validation was made against more geometrically realistic models allowing conclusions to be drawn on the appropriateness of the simplified model for clinical use.

Chapter 4 presents the development and analysis of a 3D FE model that combines mesoscale bone parts with microscale soft tissue parts. The results were validated against both the findings of previous studies and the simplified geometry model. Due to the extensive nature of the modelling process, a large part of the chapter is dedicated to presenting the modelling method (see sections 4.2 and 4.3). After assessing the validity of the model, an analysis was carried out to determine the locations of peak stresses and strains within the individual knee joint components. This included investigating the interaction between the femur and femoral cartilage in terms of propagation of OA damage.

Chapter 5 presents the main findings of the dissertation and the associated conclusions. Finally, in Chapter 6, the prospects of future study along with recommendations for future modelling endeavours are discussed.

CHAPTER 2 LITERATURE REVIEW AND RESEARCH METHODS

2.1 Osteoarthritis in the Knee Joint

OA was originally known as 'wear and tear' arthritis due to the belief that it resulted from the prolonged use of the knee joint. It is now known that the disease has a far more complex story than this with both degradation and healing in the joint leading to the overall health state of the joint. It has been estimated that 9.6% of men and 18% of women over the age of 60 years suffer from some level of OA (Woolf & Pfleger, 2003).

In recent times, there has been a gradual shift from an articular cartilage-centred view towards consideration of the entire knee joint as a system of OA degradation (Lories & Luyten, 2011). This section of the study explores both the clinical and engineering research into the pathways of OA damage within the knee joint. More specifically, the effects of femur degradation and growth on the soft tissue and degradation of the soft tissue itself has been studied and validated against clinical observations. The *in vivo* assembly of these components are shown in Fig. 2.1. The existing literature often makes use of observing the locations on the soft tissue that experience the highest stress and strain concentrations, so that conclusions can be drawn on the pathways of OA progression (Boyd, Zavatsky & Gill, 2016; Halonen et al., 2013). The general directional planes used in existing studies are shown in Fig. 2.2. These will be adopted for the present study
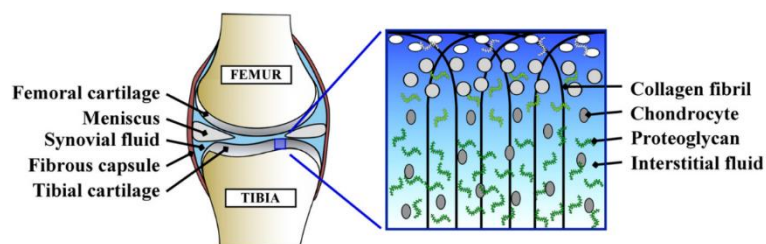
Figure 2.1 Schematic of a sagittal view of the knee joint highlighting the depth-wise view of articular cartilage composition and the varying fibril orientation (Mononen, 2013).
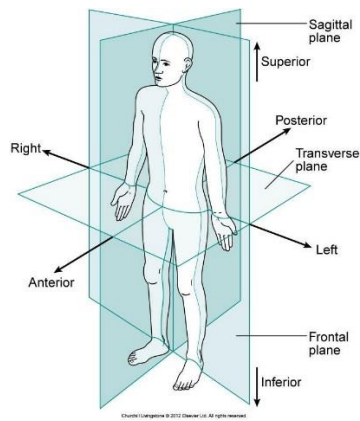
Figure 2.2 Associated directional planes for in vitro modelling. (StudyBlue)

2.2 Mechanical Properties of Bone and Soft Tissue Associated with the Knee Joint

2.2.1 Subchondral Bone

The knee joint is positioned between the upper leg bone (the femur) and the lower leg bone (the tibia and fibula). Articular cartilage at the joint is attached to the condyle surfaces of the femur and tibia (Fig. 2.1). The bone, which is significantly stiffer than the soft tissue, is often modelled as a rigid body in computational studies where the focus is on the mechanical behaviour of the soft tissue only, however, for the aforementioned reasons this is not the case in the present study. The bone architecture associated with the knee joint is considered to be a complex hierarchical composite (Reznikov, Shahar & Weiner, 2014) made up of two sub-types of bone; porous trabecular bone and dense cortical bone.

During level-standing bodyweight loading, forces are transferred through the entire knee joint and down into the tibia. It should be noted the fibula does not carry any significant loads in this particular scenario and as such, shall not be included in the modelling of the present study. Both the femur and the tibia have developed to articulate at the knee joint and can adapt in both alignment and structure to support the applied load in the most efficient manner (Toridis, 1969). Both misalignment and structural changes have been examined in the present study.

Turner et al. (1999) suggested linear isotropic material properties of $E = 1800\ MPa$ and $v = 0.3$ for both trabecular and cortical bone. This was established using nanoindentation tests where the degree of anisotropy was found to be similar to that determined by acoustic microscope investigation which suggested the obtained values were suitable for use in the future studies.
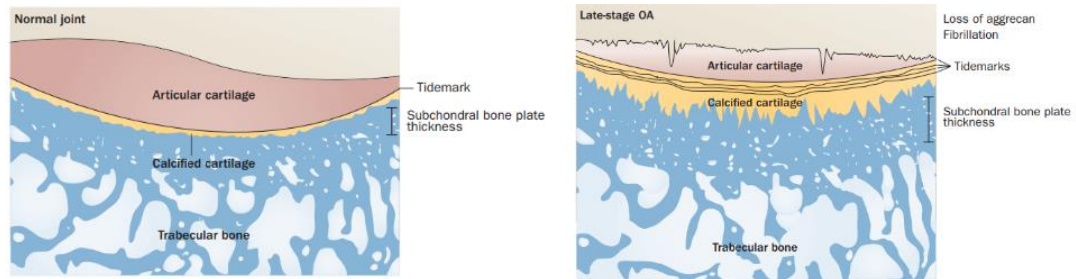
Figure 2.3 Cross-sectional schematic of a normal knee joint (LHS) and a damaged knee joint indicative of late stage OA (RHS) (Burr & Gallant, 2012)

Figure 2.3 highlights the transition from the inner trabecular bone to the outer cortical bone in both a healthy and damaged knee joint. It is seen that the bone and cartilage density decreases as OA progresses. The effects of this on the biomechanics of the knee joint and the implications for clinical treatment are investigated in Chapters 4 and 5 of this dissertation.

2.2.2 Articular Cartilage

Articular cartilage in the knee joint acts to facilitate smooth articulation and contributes towards the transfer of load. The properties of articular cartilage are continually changing with degradation, synthesis and transport of extracellular matrix (ECM) constituents, all of which can occur simultaneously. More precisely, the depth-dependent Young's modulus of cartilage is predominantly controlled by the PG content (proteins that are heavily glycosylated) while the radial deformation is predominantly controlled by the collagen fibril network (the main structural protein found in connective soft tissue).

The two-main load-bearing components are type-II collagen and PG aggrecan (Eyre, Weis & Wu, 2005). As such, articular cartilage is a multi-component soft tissue (Heinegard, 2009) with inhomogeneous properties (Schinagl et al., 1997). In this study, the validity of both homogeneous and inhomogeneous models has been compared to establish the appropriateness of increased computational demand.

2.2.3 Menisci

The knee joint menisci consist of two compartments situated between the femur condyles and the plateau of the tibia on both the lateral and medial sides. The menisci are considered fibro-cartilaginous soft tissue and have a relatively poor healing rate (Guo, Maher & Spilker, 2013). Both of the menisci horns are wedge-like semi-lunar shaped and much like the articular cartilage, they have more than one function. The menisci act as shock absorbers, load distributors and joint stabilisers (Mononen et al., 2012) and are stiffer than articular cartilage.

2.3 Computational Modelling of the knee Joint

2.3.1 Early Models

Some of the earliest representations of musculoskeletal kinematics were proposed by Borelli (1680) where particular focus was made on the spine. Following the work of Borelli, still before the existence of computational software, hand conducted stress analysis of bone was conducted. Naturally, this was a tedious process and in one study (Koch, 1917), extensive stress analysis of the femur took approximately 4 years to complete.

The FE method was introduced by Clough (1960). Early FE studies into the biomechanics of the knee joint relied on modelling the soft tissue components as viscoelastic (Rybicki, Simonen & Weis, 1972; Hayes & Mockros, 1971) and using 2D stress fields for bone parts such as the femur. However, these models did not fully portray the behaviour of the soft tissue (Mow, Kuei & Armstrong, 1980). It was realised that to comprehensively model the soft tissue, consideration of the interaction between the ECM and the interstitial fluid had to be made (Cortez, Completo & Alves, 2016).

This interaction was adequately simulated by the use of biphasic, also known as poroelastic, models which consisted of a solid and fluid phase. These models could be readily compared against experimental results (Mow, Holmes & Lai, 1984). Mow, Kuei & Armstrong (1980) produced a biphasic model of articular cartilage where the soft tissue matrix, represented by the solid phase, was saturated by synovial fluid, represented by the fluid phase. This proved a closer simulation of the actual scenario within the knee joint and as such became the standard for future studies.

A limitation of the earlier models was the applied restraint against rotation as used in studies such as Bendjaballah, Shirazi-Adl & Zukor (1995). Actual knee joints experience a variety of articulations and as such, simple one degree of freedom (DOF) models fail to adequately portray the true mechanical response. This leads to abnormal motion (Andriacchi et al., 1983). Donahue et al. (2002) found a 19% change in displacement when comparing a multiple DOF models to existing fixed-rotation models which highlighted the importance of careful boundary condition assignments. The present study set out to build upon this finding by conducting rotational analysis of the joint.

In recent years the importance of including PG and collagen fibril effects within the soft tissue parts of FE models has been recognised (Wilson et al., 2004). For this reason, PG and collagen fibril representation has been included and assessed in the present study. Additionally, there is now a preference for using geometry and material properties obtained from medical imaging for FE microscale modelling (Hambli, Bettamer & Allaoui, 2012). This will also be examined in the present study.

2.3.2 Femur Finite Element Models

2.3.2.1 Macroscale

A continuum model is considered macroscopic when the solid element size is larger than the *in vivo* structural components, that being in this case, the trabeculae (small struts of bone) (Phillips, 2012). The material properties of macroscale models are based on a combination of computed tomography (CT) scans and empirical investigation (Helgason et al., 2008). This method of modelling was used in the study by Beaupre, Orr & Carter (1990).

In macroscale models the bone is represented as a solid continuum, as such the accuracy of results when using macroscale models is reduced. This is partly due to the treatment of trabecular bone as isotropic which does not truly reflect the *in vivo* properties (Phillips, 2012). Further studies have been able to successfully extend the complexity of material properties to include orthotropy and anisotropy in both two-dimensional and 3D models of the femur (Geraldes & Phillips, 2014), as such the present study aimed to do the same.

2.3.2.2 Microscale
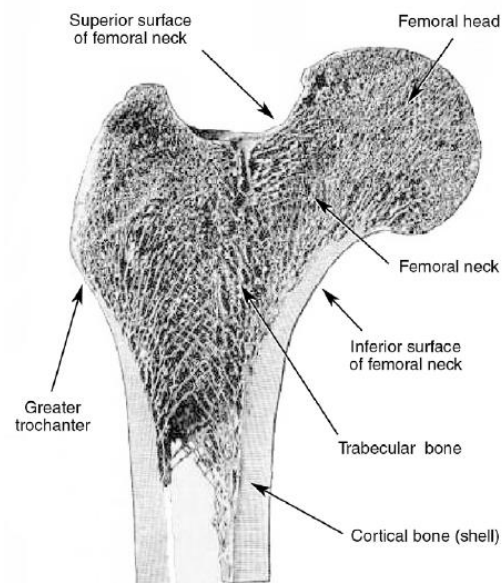
Figure 2.4 Anatomy of the proximal femur showing the composition of cortical and trabecular bone. (Voo, Armand & Kleinberger, 2004)

Another approach to FE modelling of the femur is Microscale modelling. A continuum model is defined as microscopic when the solid element size is smaller than the size of in vivo structural components, such as the trabeculae. Here, the bone geometry is derived from micro-magnetic resonance imaging (µMRI) scans and distinct material properties are assigned to the cortical and trabecular bone (Verhulp, van Rietbergen & Huiskes, 2006). An illustration of these two bone types in the femur is shown in Fig. 2.4. Micro-computerised tomography (µCT) scans are also used, however, the significant radiation dose associated with them limits their use on patients. It should be noted that homogeneous material properties of the femur are also commonly adopted. This can be a necessary adaptation due to high computational demand of microscale models due to the fine resolution of the bone.

Only a small number of studies have used microscale modelling to investigate the biomechanics of the femur and in turn the knee joint (Boyle & Kim, 2011). Although limited due to high computational demands, microscale approaches provide a basis for multiscale modelling approaches such as that of Phillips, Villette & Modenese (2015). Here, the advantage of having accurate trabecular bone trajectories, as found in microscale models such as that by Boyle & Kim (2011), is the combination of improved accuracy over macroscale models.

2.3.2.3 Mesoscale

Phillips, Villette & Modenese (2015) showed that a mesoscale FE model comprising truss and shell elements for trabecular and cortical bone, respectively, can be used to adequately represent the observed structural architecture of the femur without compromising computational efficiency. Here it was found that the structural model reduces the computational running time of analysis by over a thousand-fold. Furthermore, van Lenthe, Stauber & Muller (2006) produced a structural model, using small groups of beams to represent trabecular bone, along with a continuum model of bone.

In the case of the present study, a mesoscale FE model of the femur will be combined with microscale-poroelastic articular cartilage and menisci parts to produce an integrated computational model of the knee joint. Multiscale models, such as the one of the present study, have been attempted in recent studies (Kowalczyk, 2010; Coelho et al., 2009) where displacement distributions at the macroscale are used to drive modelling algorithms at the microscale.

2.3.3 Articular Cartilage Modelling

It has been found that PG mainly resists cartilage deformation during static compression while the collagen network governs both the compressive and tensile stiffness of the material (Hascall, Luyton & Plaas, 1990). The content of PG and collagen has been found to increase towards the cartilage-bone interface in the 'deep layer' of the soft tissue (Mow & Guo, 2002). This effect can be modelled using a depth-dependent Young's modulus property (Saarakala et al., 2010).

Another modelling consideration that should be made is the changing orientation of collagen fibrils through the depth of the soft tissue (Benninghoff, 1925). The arcade-like nature of the fibrils can be modelled by assigning spring elements between nodes to represent the fibril action (Halonen et al., 2013). The assignment of spring elements is explored in more depth in Chapter 3. Wilson et al. (2004) established a noticeable degree of difference in the mechanical response between nonfibrillar and fibrillar FE model matrices which highlights the importance of including fibril action

As FE software became more powerful, 3D knee joint models were produced which allowed greater exploration into the failure sites of cartilage. This was done by Donahue et al. (2002) who modelled the articular cartilage component as linearly elastic, homogeneous, and isotropic. Following this, 3D poroelastic analysis became prominent in the field of study, with improved correlation with experimental data being found when specifically modelling the soft tissue as poroelastic (Mononen et al., 2011).

Experimental testing has shown the highest strains in soft tissue to occur in the superficial zone, which is known to be the least stiff zone, while the lowest occur in the deep zone, which is known to be stiffest zone (Schinagl et al., 1997). It follows that a valid FE model should produce similarities to this finding.

2.3.4 Full Knee Joint Models

Recent FE studies have made use of more powerful FE elements that allow for a more comprehensive analysis of the entire knee joint (Boyd, Zavatsky & Gill, 2016; Donahue et al., 2002). The addition of more powerful elements allows for both the femoral and tibial cartilage parts to be analysed simultaneously. For example, C3D4 (4-node linear tetrahedron, coupled displacement – pore pressure tetrahedral) elements can now be utilised. This element type allows irregular geometries such as that of the femur to be adequately meshed (Boyd, Zavatsky & Gill, 2016).

There remains a gap in the literature for creating full, 3D, poroelastic FE models. In response to this, the current study attempts to harmonise 3D elastic and simplified poroelastic models. It should be noted that Mononen et al. (2012) produced a 3D poroelastic model, however, it only included the cartilage and menisci whereas the present study seeks to model the entire knee joint, bone included.

2.4 Bone Adaption Modelling

As previously mentioned, both the femur and tibia contain cortical and trabecular bone. The thickness, topology and concentration of each of these sub-types of bone are known to actively change over time with respect to the patient-specific load carrying requirements. Bone remodelling presents on a cellular level and has been reduced to the actions of the following cell types; osteoclasts, osteoblasts and osteocytes. More precisely, the osteocytes act as 'mechanostat' that responds to loading by sending signals to the other two cell types (Rucci, 2008). In other words, inactivity leads to a decrease in bone density and vice versa.

Mechanostat action can be thought of as bone reabsorption of the cortical and trabecular bone when bone experiences low strains with sufficient regularity along with bone growth when bone experiences high strains with sufficient regularity (Frost, 2003). A detailed schematic of this process is presented in Fig. 2.5. The full process of mechanotransduction remains to be clarified (Rucci, 2008).

Bone adaption FE modelling has been explored in previous studies (Phillips, Villette & Modenese, 2015; Phillips, 2012) where shell and bar elements were varied based on nodal connectivity, element size and element distribution.
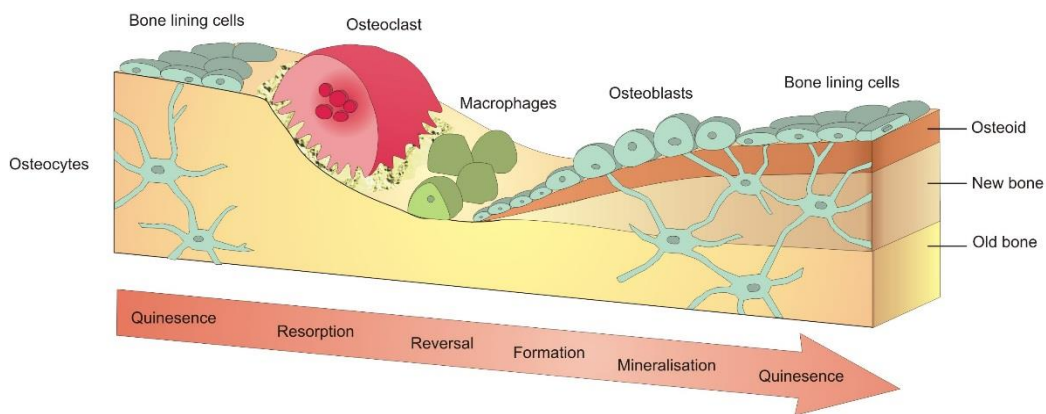
Figure 2.5 Detailed representation of the bone remodelling process (Biomedical Soft Tissue Research, University of York).

In summary, the literature presents evidence that in order to effectively model the biomechanics of the knee joint, consideration of the full geometric irregularities and material properties must be included to produce results in accordance with experimental data. Furthermore, bone should preferably be modelled as anisotropic opposed to isotropic. This can be achieved through the implementation of a bone adaption algorithm. It has also been established that OA is not simply a disease confined to degradation of articular cartilage but is rather a disease of the whole knee joint with a complex pathology. It follows that further refinement of modelling methods is required to better understand the disease and its effects. In addition, it has been noted that multiscale models allow for reduced computational demand while maintaining an acceptable level of accuracy.

CHAPTER 3 DEVELOPMENT OF PROTEOGLYCAN CONTENT AND COLLAGEN FIBRIL MODELLING

3.1 Introduction

In this section, the importance of the collagen fibril network arrangement and the PG content in articular cartilage has been investigated using a simplified-geometry knee joint model. Specifically, analysis of depth-dependent collagen fibril orientation and PG content has been conducted. Although the main aim of this project was to produce a full 3D knee joint model, the simplified representation was deemed an acceptable starting point for validating the underlying modelling assumptions and to allow later comparison of results to the 3D model. Both healthy and damaged model cases have been analysed.

The modelling assumptions are as follows:

- The mechanical property changes through the cartilage thickness are represented by partitioning the thickness into four layers. In reality, the properties will have a smoother variation through the depth.
- Collagen fibrils can be idealised as parallel to the cartilage surface in the superficial layer and perpendicular to the cartilage surface in all other layers. In reality, they take an arcade-like form.
- A fixed boundary condition can be given to the bottom surface to represent the level-standing restraint experienced by the tibia.
- Negligible fluid transfer takes place between the bone and soft tissue; hence the bone is modelled as elastic, i.e. the bone has been modelled as macroscale. The assumption of negligible fluid transfer is supported by the findings of Maroudas et al. (1968) where negligible fluid transfer was found at the bone-cartilage interface.
- In the soft tissue model parts, only the permeability has been altered to indicate severe OA damage. As previously mentioned, in reality OA is believed to alter the properties of the entire knee joint. This will be further investigated in later chapters where the 3D geometry model is used.

3.2 Geometry
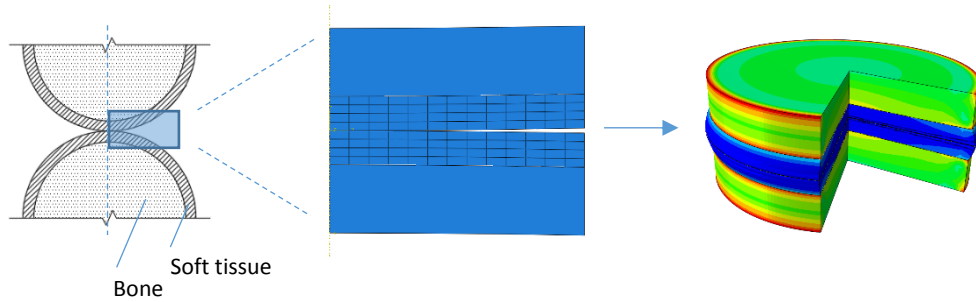
Figure 3.1 LHS: Schematic of the two cylindrical parts used to model the femur-tibia contact. Middle: Axisymmetric plane showing the four layers of the articular cartilage (from the free edge to the bone surface: superficial, second, third and deep layer). RHS: Swept plane showing the Von Mises Stress (VMS) distribution for the entire simplified geometry model.

The axisymmetric plane was modelled using Abaqus/Standard 2016 and is shown in Fig. 3.1. Both the femur-to-femoral cartilage and tibia-to-tibial cartilage parts were modelled as arc segments from a circle of radius 400 mm, this was based on the simplified geometry assumptions of Federico et al. (2004). By doing so, the model simulates the rolling-like contact between the femoral and tibial condyles at the knee joint while maintaining computationally efficiency. The cartilage parts are both 1 mm thick while the bone parts are both 2 mm thick.

3.3 Materials

The elastic depth-dependent properties of healthy knee joint model were taken from Schinagl et al. (1997) while the permeability properties were taken from Julkunen et al. (2008). On the recommendation of Federico et al. (2004) the damaged knee joint was modelled using an initial permeability value of double that of the healthy cartilage. The material properties are summarised in Tab. 3.1. The Young's modulus assignment for each layer was used to represent the PG distribution while the permeability assignment enabled a poroelastic analysis to be conducted.

To model the effects of the collagen fibril density, spring elements were added between nodes of the continuum elements as shown in Fig. 3.2. Only the superficial layer was assigned springs that were placed parallel to the cartilage surface, i.e. in the horizontal direction. This is due to the arcade like nature of the fibril network as shown in Fig. 2.1. The collagen fibrils carry the load primarily in tension, hence their effect is negligible in the lower layers when the cartilage is subjected to an axial load as the bulk of the fibres are oriented perpendicular to the cartilage surface. The stiffness and damping coefficient of the inter-nodal springs were also taken from Julkunen et al. (2008).

Table 3.1 Material properties assigned to the healthy model (Wilson et al., 2003). (a)(Cohen, Gardner & Ateshian, 1993); (b) (Chern et al., 1990): (c) (Turner et al., 1999). [†] Superficial layer, layer 2, layer 3, deep layer.

	Articular cartilage *(a)*	Menisci *(b)*	Bone *(c)*
Young's modulus E [MPa]	0.11, 0.51, 0.37, 0.84 [†]	28	1800
Poisson's ratio v [dimensionless]	0.018	0.36	0.3
Permeability k_0 [10^(-15)m^4/Ns]	3	1.26	-
Solid volume fraction n [dimensionless]	0.25	0.75	-
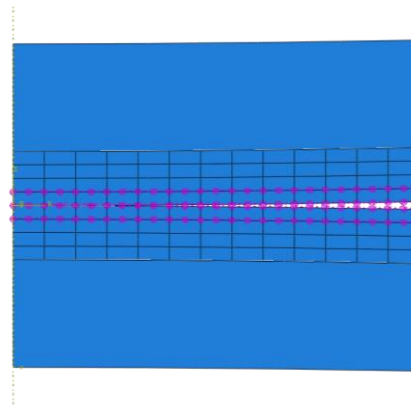
Figure 3.2 Arrangement of inter-nodal springs in the superficial layers, representing the collagen fibril effects. Note: the nodes highlighted purple represent the attachment points of the spring features.

The permeability of the model was assumed to be strain-dependent due to the cartilage permeability reducing during the loading period. This was found to be an appropriate assumption by Lai, Mow & Roth (1981). The change in permeability with respect to the void ratio is given below (Prendergast, Van Driel & Kuiper, 1996):

$$k = k_0 \left(\frac{1 + e}{1 + e_0} \right)^M$$

<div align="right">(3.1)</div>

Where the constant $'M'$, equals 7.1 (Wilson et al., 2004) and the initial void ratio $'e_0'$, equals 4 (Wilson et al., 2003). From here the change in permeability with the decrease in void ratio was calculated in a tabular form and then implemented into the property definition of the soft tissue parts.

3.4 Loading, Amplitude and Step Assignment

A 300 second 'soils' analysis-step was used to simulate the poroelastic response of the cartilage component of the model. A displacement of 0.3 mm was applied linearly over the first 10 seconds of the step and then held constant for the remainder of the step. An initial gradual application of load was used to aid the convergence ability of the simulation.

This analysis scenario was chosen to represent level-standing for a period of 5 minutes, allowing the stresses and strains within the bone and soft tissue to be clearly observed. Furthermore, the results could be validated against Federico et al. (2004) where a similar model and loading condition was used.

3.5 Boundary Conditions
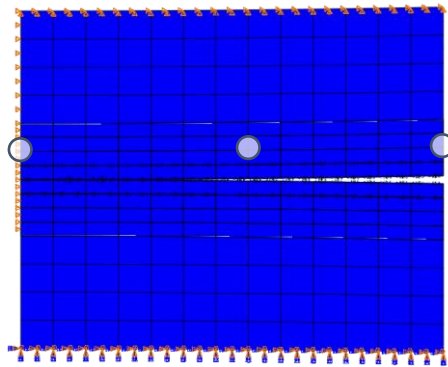
Figure 3.3 Boundary conditions on the axisymmetry plane of the simplified model. The white circles highlight the nodes used for length-dependent analysis. These are, from left to right: the centre, middle, and end node.

Figure 3.3 shows the loading and boundary conditions on the axisymmetry plane of the model. The tibia part was fixed on its bottom side to represent its stationary positioning during the loading. The left-hand side of the plane, that is the line of axisymmetry, was restrained in all DOFs except that of vertical movement to allow for simulation of the compression of the bone and soft tissue.

Naturally, the pore fluid required an escape path to model the sponge-like response of the cartilage when under the applied displacement. To do this, the free surfaces of the opposing soft tissue parts were assigned a zero-pore pressure value in the initial step. Physically, this represented the synovial fluid escaping into the synovial joint casing.

Two additional boundary condition assignments were the initial pore pressure and void ratio throughout the model at the start of the analysis. The pore pressure was chosen to be 0.1 MPa and the void ratio 4, both of which were assigned over the entire body of the soft tissue parts. These values were implemented using the predefined field feature in Abaqus/Standard 2016.

3.6 Meshing

For the bone parts in the model, CAX4R (4-node bilinear axisymmetric quadrilateral, reduced integration, hourglass control) (Fig. 3.4) elements were used. Due to the use of reduced integration the elements are considered less accurate than the full integration counterpart elements. For the soft tissue parts of the model, CAX4P (4-node axisymmetric quadrilateral, bilinear displacement, bilinear pore pressure) (Fig. 3.4) elements were used to simulate the pore pressure response on and within the soft tissue. Both element types are available within Abaqus/Standard 2016 and are shown below.
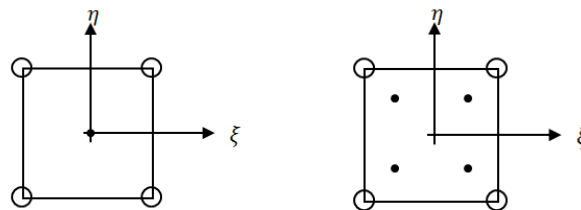
Figure 3.4 LHS: CAX4R element used for the bone meshing (Note: only one integration point is used). RHS: CAX4P element used for meshing of the tissue (Note: four integration points are used).

3.7 Results

3.7.1 Biomechanical Response of the Healthy Model
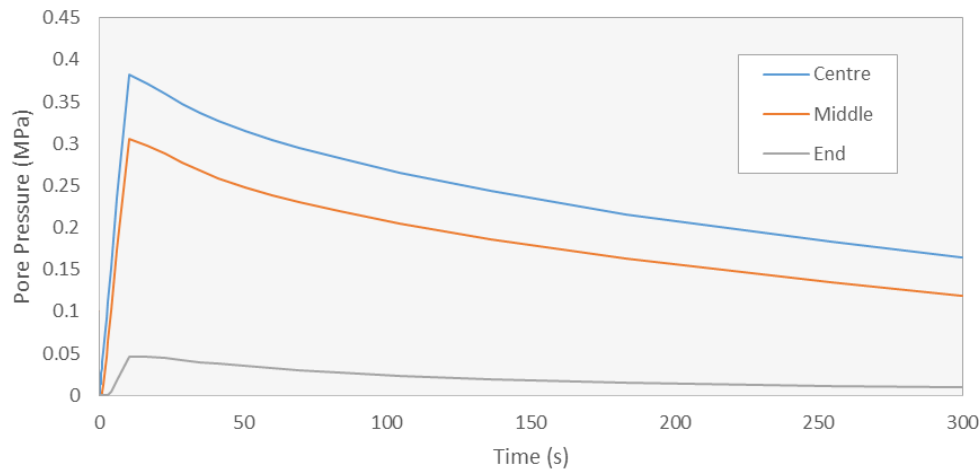
Figure 3.5 Pore pressure during loading of the femoral cartilage at different nodal locations along the length.

It can be seen in Fig. 3.5 that the end region of the cartilage component had the smallest initial pore pressure rise, this was due to the pore fluid having the shortest path to the escape boundary region at this point, meaning the fluid dissipated before the pressure could develop. The centre region, the inner most region, had the greatest initial pore pressure as the pore fluid had the longest path to the escape surface at this location

Over time the pore pressures at all locations along the radial direction of the cartilage tended towards similar values which was due to the biomechanical system finding an equilibrium between the solid and fluid phase with relatively small fluid dissipation across the cartilage now occurring.
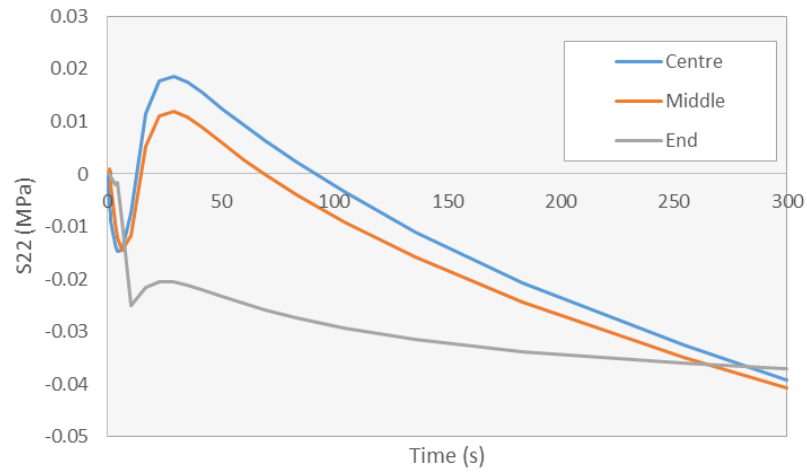
Figure 3.6 Vertical stress response during loading of the femoral cartilage at different node locations along the length. Note: compression negative, tension positive.

Figure 3.6 highlights the end region as having the greatest initial compressive stress rise due to the quicker dissipation of pore fluid. This resulted in the solid phase carrying more of the load induced by the displacement. It was also found that the initial increase in stress of the solid phase was followed by a decrease in stress. This phenomenon results from the sponge-like effect of the fluid phase where the initial stress in the solid material is transferred to the fluid. The solid then increased in stress as the pore fluid dissipated leaving only the solid to carry the load.

Over time the stresses tended towards the same value across the radius of the soft tissue. This was due to same reason as the pore pressure value tending towards uniform distribution, as mentioned previously.

3.7.2 Comparison of the Healthy and Damaged Model
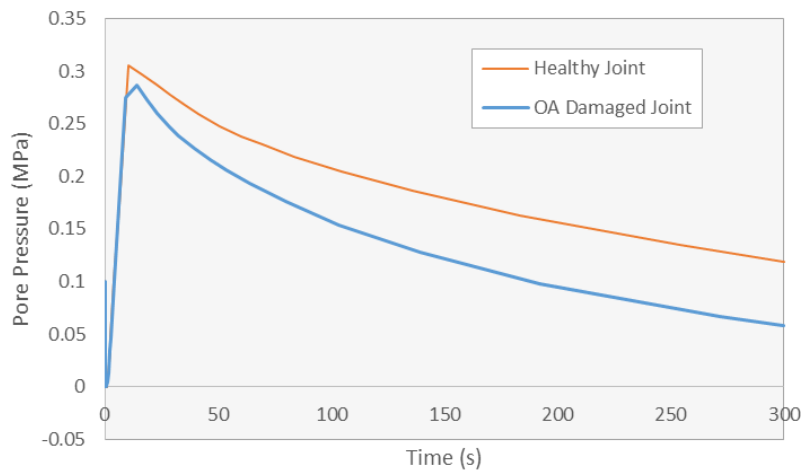
Figure 3.7 Comparison of the pore pressure response at the middle node of the femoral cartilage between the healthy and damaged model.

Figure 3.7 shows that the OA damaged has a slightly slower initial pore pressure rise. This was due to the increased permeability definition resulting in faster dissipation of the pore fluid from the soft tissue parts. Maximum pore pressures of 0.31 MPa and 0.29 MPa are reached in the healthy and OA models, respectively.
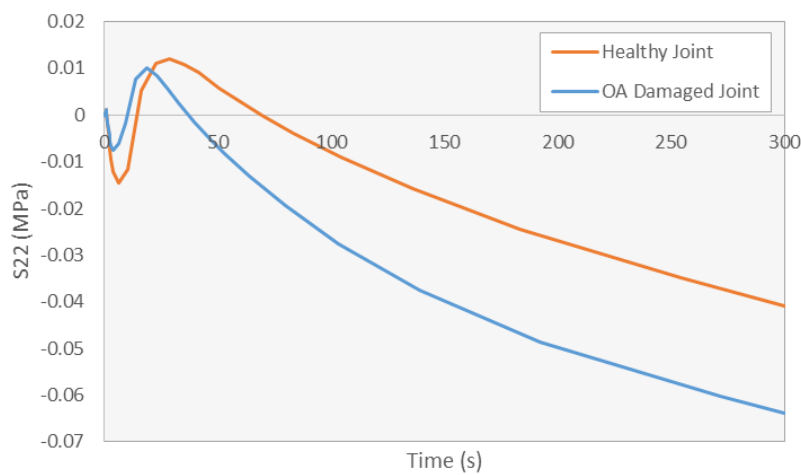
Figure 3.8 Comparison of the vertical stress response at the middle node of the femoral cartilage for both the healthy and damaged model.

36
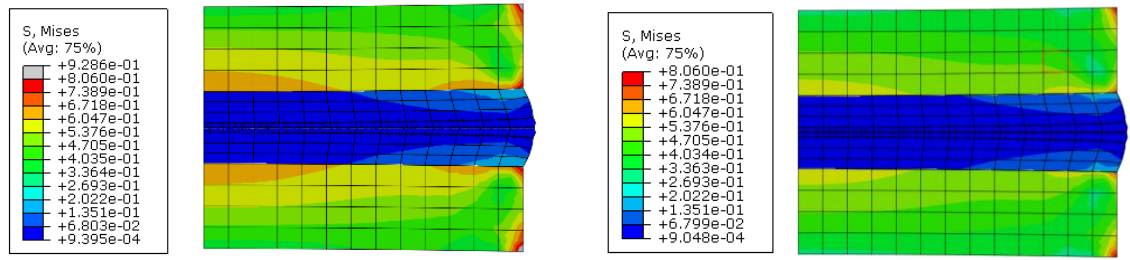
Figure 3.9 VMS contour plot at 10 s into the analysis (point of full displacement application) on the healthy model (LHS) and the OA model (RHS).

For the majority of the 5 minute loading condition, the OA damaged model experienced greater vertical stress due to reduced pore fluid content caused by the increased permeability of the cartilage layers (Fig. 3.8). Physically, this represents the loss of both the PG content and collagen fibril content due to soft tissue degradation.

To further analyse the model, contour plots of the VMS distribution across the axisymmetric plane were produced (Fig. 3.9). Greater stress throughout bone in the healthy model was found. This results from the smaller initial permeability value which reduces the damping effect on the bone movement from the soft tissue below. In other words, the stresses within the bone develop faster while the stresses within the soft tissue develop slower, for the healthy model.

3.8 Discussion

3.8.1 Validation of Results

The results presented above were compared against the study of Federico et al. (2004). Here similar results were found in terms of the response of the bone-soft tissue model for both pore pressure.

Federico et al. (2004) found that upon linear application of the displacement, over the same time step as used in the present study, the pore pressure at the same centre node location as used for the present study reached a maximum value of 0.85 MPa at 10 s. In the present study, the maximum pore pressure was found to be 0.38 MPa also after 10 s. The difference in magnitude most likely results from the use of more realistic stiffness properties of the cartilage in the present study. Federico et al. (2004) did not use depth-dependent stiffness properties for the soft tissue components or spring elements to model collagen fibrils, both of which reduce the load initially carried by the fluid phase and hence the pore pressure).

The stress response in the solid phase of the model was also similar to that of Federico et al. (2004) with a sharp increase in vertical stress over the first 10 s. In this prior study, the stress was then seen to decrease to the extent of going into tension. As mentioned, this is due to the relationship of the solid and fluid phase where the fluid phase takes over the load carrying at this point of the loading condition. Following this, the stress gradually increased to a final value of -0.01 MPa at 300 s, this is compared to -0.04 MPa at 300 s in the present study. The difference in magnitude is for the same reason as was discussed previously for the pore pressure difference between the two studies. This represented the solid phase taking over the load carrying response as the fluid gradually dissipates from the cartilage, much like in the present study.

3.8.2 Limitations

To accurately model stress distribution and concentration throughout the various components of the knee joint, the full 3D-complex geometry must be modelled. This allows patient-specific regions in the knee joint that are prone to OA damage to be adequately identified and following this, suitable clinical treatment can be determined. With this in mind, the simplified geometry model used in this study is limited as the stress results are likely to concentrate in different areas from the *in vivo* scenario.

A further limitation is an axial load, applied as a displacement over the top surface of the model, is not characteristic of true forces acting on the joint during level-standing for a fully extended knee joint. Ideally, the full femur should be modelled so to include the joint contact (JCF), abductor muscle (ABD), and iliotibial band (ITB) forces applied at the head and greater trochanter of the bone (Fig. 3.10). These forces should be appropriately adjusted for their action at the knee joint.
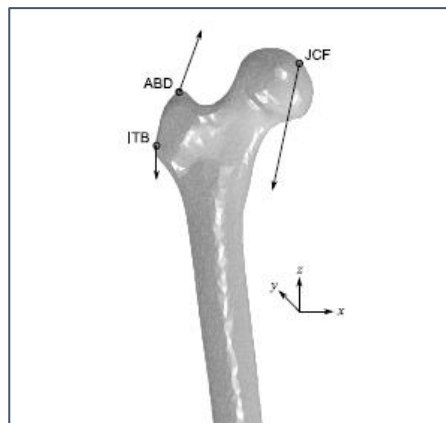
Figure 3.10 Idealised femur forces (Imperial College London, Structural Biomechanics Group).

In the simplified geometry model, the collagen fibril orientations are assigned in parallel and perpendicular directions from the cartilage surface. In reality, the fibrils take an arcade-like form and are made up of a diverse network of interlocking strands. Further, in this model, the fibrils are defined between nodes when in reality, they will be spaced on a microscopic scale.

Additionally, the defined layers of cartilage are not so pronounced in actual cartilage. The true scenario has a smoother transition between different stiffness layers and as such the simplified geometry model assumption of four distinct layers is limited in this sense. Furthermore, individual fibril interaction and fibril-to-PG interaction has not been considered. Again, this is an important characteristic of the knee joint and as such should be included in computational simulations in order to fully understand the biomechanical behaviour of the joint.

A final important limitation to note, is that the fibril definitions of the model only consider the tensile response. Actual fibrils have a complex response to everyday loads where compression and buckling behaviour also arises. As such, the results of the simplified model are likely to have a certain degree of dissimilarity when compared to *in vivo* test findings.

3.9 Conclusions

The analysis of the model presented in this chapter produced the following conclusions about the biomechanical behaviour of the knee joint in both healthy and OA damaged states:

- Upon application of a bodyweight load, via an applied displacement, the inner region of the soft tissue experiences the greatest initial pore pressure rise but the lowest vertical stress in its solid phase.
- After a prolonged period, that is a period greater than 5 minutes, both the pore pressure across the soft tissue parts and the stress across all parts of the model reach uniform values. It can be said that the joint model is capable of reaching mechanical equilibrium.
- To fully understand the onset and development of OA, more detailed and patient-specific analysis of everyday loading conditions and knee joint arrangements are required.

- The simplified geometry model provides a fast and effective foundation for computational investigation of the mechanical behaviour of the knee under basic loading conditions that presents characteristics of degradation.
- The simplified geometry is effective in terms of modelling the PG and collagen fibril effects. This is due to the relative ease in partitioning the individual joint components to assign depth, and potentially width, dependent material properties along with applying spring elements, representing collagen fibrils.

CHAPTER 4 DEVELOPMENT OF THE MULTISCALE FINITE ELEMENT THREE-DIMENSIONAL KNEE JOINT MODEL

4.1 Introduction

As discussed in Chapter 2, microscale models of bone often prove too computationally expensive and as such mesoscale models can be used to mitigate this problem while having an acceptably small impact on the accuracy of the bone model. It naturally follows that a single model of the entire knee joint can be produced using mesoscale bone parts combined with microscale soft tissue parts. The aim of this chapter was to create a full 3D FE model of the knee joint using mesoscale femur and tibia parts, making use of an adaptive bone algorithm to improve the bone characteristics, and microscale cartilage and menisci parts. This is termed a multiscale model.

In addition to the above, by modelling the entire geometry of the knee joint in a single model it was hoped that light would be shed on the pathways of OA damage as a disease of the entire joint instead of simply confining the disease to individual joint components. To do this, degradation properties were considered in both the bone and soft tissue components of the model. Following this, concentrations of stress and strain in important locations of the bone and soft tissue were examined along with the change in pore pressure response of the soft tissue under varying load conditions and material properties.

To investigate the effectiveness of the multiscale model, comparison was made against the results of previous studies and the simplified geometry model presented in Chapter 3. Furthermore, this method of knee joint modelling has been used to address the shortcomings in previous studies, specifically in terms of computational limitations.

4.2 Bone Adaption Algorithm

As previously mentioned in Chapter 2, the bone associated with the knee joint has a composite network of cortical and trabecular bone material. To model this network within an FE model of the knee joint, a combined MATLAB and Python (Python Software Foundation) script was implemented. This script utilises the mechanostat theory presented by Frost (2003).

The algorithm adjusts the cross-sectional area and thickness of the trabecular truss and cortical shell elements, respectively. Starting at an initial truss radius and shell thickness of 0.1 mm, successive iterations are run to produce an optimised arrangement of and truss and shell elements of various concentrations and sizes. Iterations cease once convergence has been achieved. Using the adaptive algorithm equations set out by Phillips (2012) and Frost (2003), presented below in Eq. 4.1, the following zones were defined to create areas of higher and lower bone density based off of the given strain ranges.

$$\phi_{i,j} = \begin{cases} 1, & \text{for } 0 \le |\epsilon_{i,j}|_{\max} \le 250\mu\epsilon & \text{(Dead zone)} \\ 1, & \text{for } 250 < |\epsilon_{i,j}|_{\max} < 1000\mu\epsilon & \text{(Bone resorption)} \\ 0, & \text{for } 1000 \le |\epsilon_{i,j}|_{\max} \le 1500\mu\epsilon & \text{(Lazy zone)} \\ 1, & \text{for } |\epsilon_{i,j}|_{\max} > 1500\mu\epsilon & \text{(Bone apposition)} \end{cases}$$

(Eq. 4.1)

To manipulate the cross-sectional area and thickness of elements, Eq. 4.2 and Eq. 4.3 were used within the adaptive algorithm script (Phillips, 2012; Frost, 2003).

$$\text{if } \phi_{i,j} = 1, \quad A_{i+1,j} = A_{i,j}\frac{|\epsilon_{i,j}|_{\max}}{\epsilon_t}$$
$$\text{else} \qquad A_{i+1,j} = A_{i,j}$$

(Eq. 4.2)

$$\text{if } \phi_{i,j} = 1, \quad T_{i+1,j} = \frac{T_{i,j}}{2}\left(1 + \frac{|\epsilon_{i,j}|_{\max}}{\epsilon_t}\right)$$
$$\text{else} \qquad T_{i+1,j} = T_{i,j}$$

(Eq. 4.3)

The script was modified for the requirements of the present study. This included; changing the node and element data sets for the shell and truss elements, changing the multi-point loads to a singular axial load (this was due to the reduced size of the femur making the multi-point load application at the head of the femur not possible) and changing the nodes of the boundary condition assignments due to the change in geometry. The node and element data sets of the present model were obtained using the structural mesh generator script discussed later in section 4.3.1.

During each iteration of the script, a bone model is simulated in ABAQUS/standard under the bodyweight loading condition. Following the final iteration, the third iteration in the case of the present study, an input file was generated for use within the complete knee joint FE model. This input file contained the element sets of the various shell and truss sizes, the shell thickness range was 0.1-8 mm while the truss radius range was 0.001-2 mm. Images of the finalised truss and shell element bone arrangement are shown in Fig. 4.1 and Fig. 4.3, respectively.
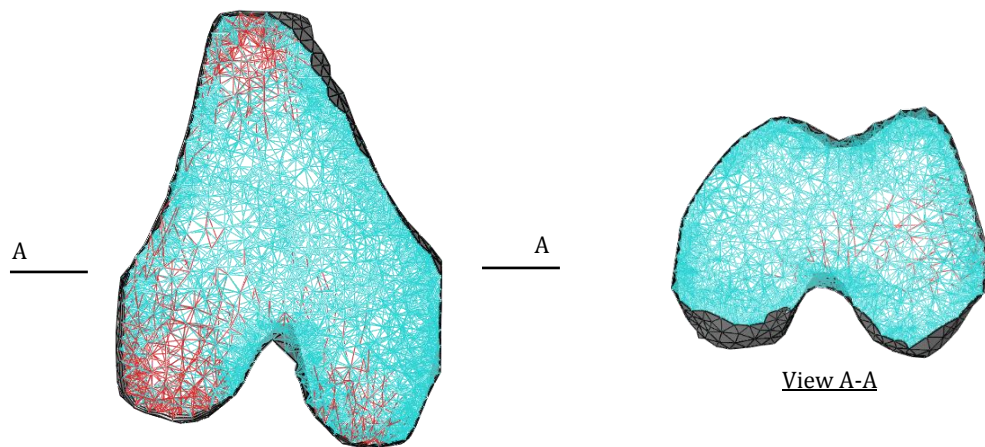
Figure 4.1 5 mm slices of the femur bone part. LHS: Elevation view. RHS: Plan view located at A-A. Note: for clarity, the shell thickness has been increased to three times the actual thickness while the truss cross-sectional areas have not been rendered. The seed size used for the shown view cuts is 4 mm.
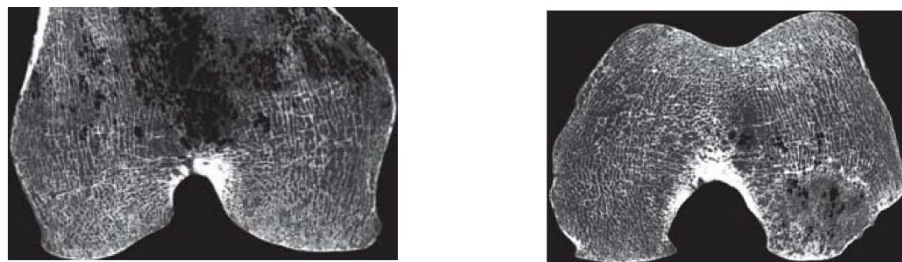
Figure 4.2 CT scans of a 5 mm femur elevation slice (LHS) and a 5 mm femur plane slice (RHS) (Imperial College London, Structural Biomechanics Group).
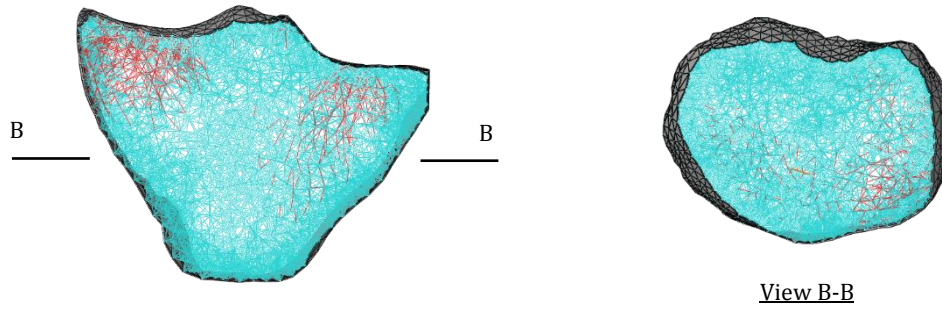
Figure 4.3 5 mm slices of the tibia bone part. LHS: Elevation view. RHS: Plan view located at B-B. For clarity, the shell thickness has been increased to three times the actual thickness while the truss cross-sectional areas have not been rendered. The seed size used for the shown view cuts is 4 mm.

The main functions of the bone generation script for the present study are as follows:

- The initial femur and tibia geometries taken from the CT scans were meshed using 4 mm edge length 4-noded tetrahedral elements within Abaqus. The node coordinates were then read and loaded into the script.
- The surrounding nodes of each individual node-point of the femur and tibia were identified. 16 surrounding nodes were identified which would go on to form the 16 truss element connection.
- The inner nodes of the bone parts were assigned truss elements while the outer faces of the tetrahedral elements were defined as triangular elements so that they could then be converted to shell elements.
- Finally, an Abaqus input file of the composite bone geometry parts was written and saved.

Following this, the bone adaption algorithm script was run, making use of the now generated initial bone parts. The main functions of the bone adaption algorithm script are as follows:

- The initial truss and shell element coordinates and inter-element connection definitions were loaded into the script.
- A disc operating system command was then used to run the Abaqus input file with a subsequent command used to extract the acquired strain data.
- The extracted strain data was organised into the shell and truss strains with section sizes for each element type being dictated by the chosen strain value ranges (Eq. 4.1) along with the establishment of the model 'dead-zones'.

- The trabecular elements were limited to a range of 0.1 mm to 2 mm. A 1 μm discrete circular cross-section was added to allow for effective removal of truss elements and to provide numerical stability. In other words, the elements are so small their effect can be considered negligible.
- Following this, a connectivity matrix was derived for the nodes.
- Low radius and low strain elements were then effectively 'removed'.
- The shell elements were confined to the range of 0.1 mm to 10 mm thickness. Unlike the truss elements, none of the shell elements were removed during the successive iterations.
- The updated Abaqus input file was then written using the new element sizes and arrangements.
- The new input file was then run for successive iterations. The script completed once model convergence was achieved based on the strain range definitions of Eq. 4.1.

Figures 4.1 and 4.3 show the concentration of trabecular truss elements towards the outer edges of the femur and tibia bone parts as expected. The radii of the blue coloured elements are in the range of (0.001 mm ≤ radius < 0.11 mm) while the radii of the red coloured elements are in the range of (0.11 mm < radius ≤ 0.81 mm). The stiffness of the truss elements below 0.1 mm in radius was considered negligible however, as noted before, their inclusion was required to achieve numerical stability. The resulting femur and tibia parts represented the most effective section for resisting the bodyweight loading condition. Mathematically, the concentration of bone area to the furthest parts away from the section centroid represents an optimised second moment of area. Areas in which less bone density is required can also be seen, physically this represents material efficiency consideration from the bone remodelling process. The correlation of the trabecular and cortical bone network with the actual femur has also been shown (Fig.4.2).
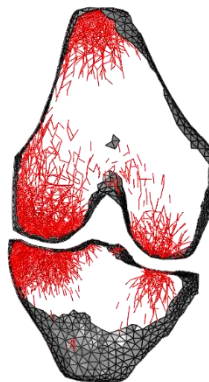
Figure 4.4 Display of truss elements greater than 0.11 mm in radius on a 5 mm slice view of the femur and tibia, after conducting the bone adaption process.

Most of the generated truss elements were less than 0.107 mm in radius. The truss elements larger than this were found to concentrate near the applied load, the main area of the lateral condyle and towards the outer shell. The generated truss adaption should be used with caution as the algorithm is highly dependent on the bone geometry and loading condition, both of which have been idealised in the present study.

4.3 Modelling Process within the Finite Element Software

4.3.1 Geometry

All the geometry parts used in the model came from magnetic resonance imaging (MRI) scans of a donor patient at the Biomechanics laboratory of the Cleveland Clinic. A 1.0 Tesla extremity MRI scanner (Orthone, ONI Medical Systems Inc, Wilmington MA) was used to create the images.

To improve the clarity of the scans the knee was placed in a fully extended position. The MRI process consisted of a 3D spoiled gradient echo sequence with fat suppression. A field view of 150 mm x 150 mm with a slice thickness of 1.5 mm was used. Scans were carried out in the axial, sagittal, and coronal planes. The purpose of using more than one plane for the scanning was to refine the images so that model geometry parts could be created using Rhinoceros (McNeel North America, Seattle, WA).

It should be noted that ligaments were not included for the bodyweight loading analysis as their contribution to the mechanical behaviour of the joint is negligible during level-standing axial loading at full-extension. Reduced femur and tibia parts have been used due to the nature of the study, this was deemed appropriate by using boundary conditions on the two parts that accurately represented the *in vivo* scenario.

4.3.2 Materials

Material properties of the soft tissue components were taken from Wilson et al. (2003). These are shown previously in Table 3.1. For the femur and tibia parts in the healthy model, a Young's modulus (E) value of 18000 MPa and a Poisson's ratio (v) value of 0.3 were assigned. This was based on the reported values for bone at soft tissue level by Turner et al. (1999).

Residual stiffness of bone can also be added to the model (E=100 MPa, v=0.3). This represents a combination of additional material within the bone not covered by the cortical and trabecular bone sets, in other words, residual material such as bone marrow. By doing this, the model output becomes significantly larger meaning sufficient computational capacity is required to make the addition. Due to this, the present studied excluded the residual stiffness consideration.

4.3.3 Loading, Amplitude and Step Assignment

A 374 N point load was assigned to a nodal point on top of the femur part based on the value used by Mootanah et al. (2014). This load represented bodyweight during level-standing passing through one leg. It should be noted that bodyweight loading is patient-specific, however, for the case of this study where the knee joint scans were taken from a 77 kg patient, 374 N was deemed an appropriate value.

To fully investigate the pore pressure response of the soft tissue components, a one-hour bodyweight loading analysis was carried out. Similar to the simplified geometry model, a 'soils' analysis-step was specified from the software user interface and an initial step size of 0.036 s was set. Due to the complexity of the model, it was found that certain surface nodes of the two cartilage parts would intersect with their corresponding contact surface. As a result, the load had to be applied slowly to prevent convergence issues. To do this a tabular amplitude was assigned to the load and relevant boundary conditions. This meant the load was applied linearly over the first second of the analysis and then held constant for the remaining time. Additionally, the maximum step time was limited to one hour while the maximum pore pressure increase between steps was limited to 10 MPa. This ensured a controlled set of results.

4.3.4 Boundary Conditions

As illustrated in Fig. 4.5, fixed restraints and vertical displacement only restraints were applied to the shell nodes on the tibia and to all the outer shell nodes of the femur, respectively. This represents the knee joint behaviour during axial loading with the leg fully-extended.

Additionally, an initial zero pore pressure boundary condition was applied to all free edges of the soft tissue elements. This represented the escape surface for the interstitial fluid. At the bone-cartilage interfaces, it was assumed no fluid can be transferred and hence fluid cannot escape (Ogata & Whiteside, 1979).

To run a 'soils' analysis-step, predefined fields had to be assigned which propagated from the initial step. A pore pressure of 0.01 MPa was assigned to all soft tissue components as an initial non-zero starting point, void ratios of 4 and 0.333 were assigned to the cartilage and menisci parts, respectively (Wilson et al., 2004).

4.4 Meshing

4.4.1 Bone Meshing

The combined shell and truss element mesh was created using the previously mentioned MATLAB R2016a script. An illustration of the shell-truss mesh system is shown in Fig. 4.5. The truss elements which have a radius of 0.001 – 0.953 mm represent the arcade-like network of the trabecular bone while the outer shell elements, seed size 4mm and thickness 0.1 – 2.274 mm, represent the cortical bone. To create an appropriate number of truss elements, each node was modelled to have 16 truss elements intersecting at it.
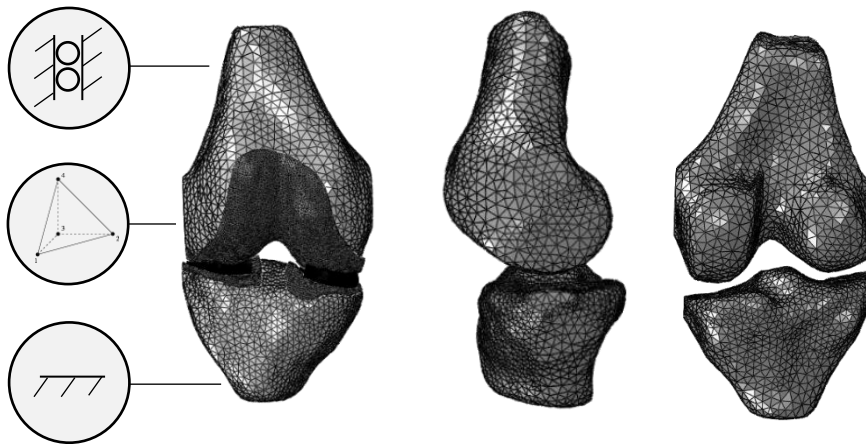
Figure 4.5 LHS: front elevation view-cut of the FE model along with the C3D4P element type used for the tissue meshing. Middle: Lateral-side elevation. RHS: back elevation.

4.4.2 Soft tissue Meshing

The soft tissue components, cartilage and menisci, were assigned a seed size of 1 mm as this enabled an appropriate number of elements through the thickness of each soft tissue component while not being unnecessarily computationally expensive. By having a minimum thickness of two elements, proper investigation of mechanical response through the soft tissue depth was enabled. C3D4P (4-node linear tetrahedron, coupled displacement-pore pressure) elements were used. An illustration of this element type along with the mesh arrangement for the entire model is shown in Fig. 4.6.

4.4.3 Mesh Sensitivity Analysis

To establish an appropriate mesh size for the femur and tibia geometries, a mesh sensitivity analysis was carried out to find the critical seed size. This seed size was chosen based on balancing computational efficiency of the model and accuracy of the provided results. Three side sizes were compared; 4 mm, 3 mm and 2 mm. The 4 mm was based on the study by Phillips, Villette & Modenese (2015) where a seed size of 3.9 mm was used for creating the volumetric mesh of the bone. To perform the mesh sensitivity analysis, maximum VMS node values were taken from the medial condyle surface of the femur geometry for each of the three models of different mesh coarseness (Fig. 4.6). Additionally, the maximum axial logarithmic strain value on the superficial surface of the medial tibial cartilage was taken for each model (Fig. 4.7).
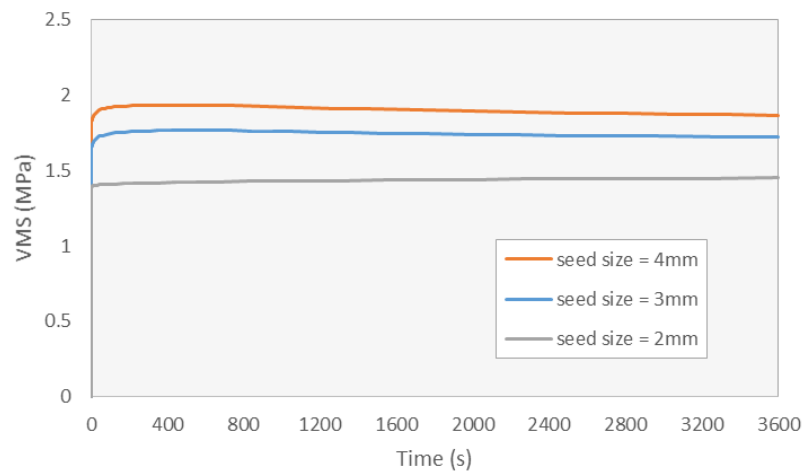
Figure 4.6 VMS mesh sensitivity plot for different seed sizes of the bone parts of the 3D knee joint model.
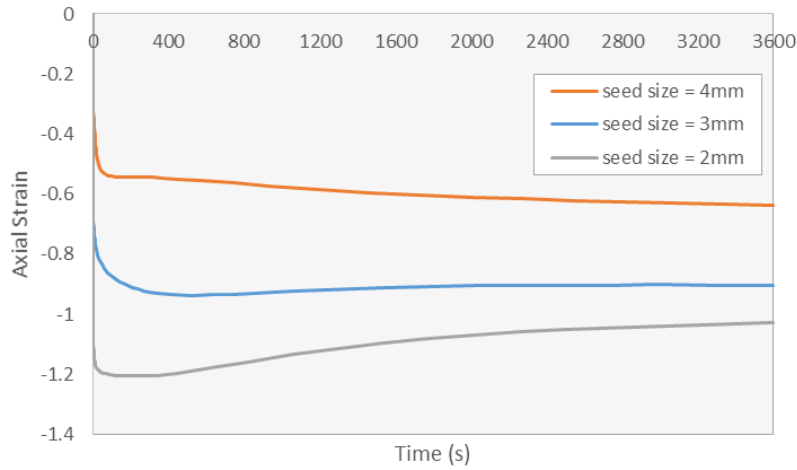
Figure 4.7 Axial strain mesh convergence plot for different seed sizes of the bone parts of the 3D knee joint model.

It can be seen from Fig. 4.6 and 4.7, that as the mesh of the femur and tibia parts is refined, the results of VMS and axial strain tend towards more realistic results. During the first second of the analysis, as the load was being linearly applied, large differences between values for the coarsest and finest seed size models were observed. These were 0.4 MPa for the VMS response and 0.68 for the axial strain. Towards the end of the analysis, the model responses approached one another with the maximum differences between models being 0.3 MPa for the VMS and 0.41 for the axial strain. The relatively large final strain difference warrants further investigation using a refined mesh and/or more powerful element types. A previous study, using the same soft tissue geometry and loading condition, showed improvement in model results when using C3D10MP (10-node modified quadratic tetrahedron, pore pressure, hourglass control) elements over first order approximation C3D4P elements (McLennan & Pankaj, 2016) , the same as which have been used in the present study. However, due to the large nodal expense of the linear approximation elements, the available Abaqus licence of the present study could not accommodate quadratic elements.

As shown in Tab. 4.1, the 4 mm seed size model ran the fastest by completing the one-hour bodyweight loading simulation with a central processing unit time (CPU) of 6491.5 s seconds (wall clock time of 3538 s, or 1.0 hr). By halving the seed size to 2 mm, the CPU time increased to 89078 s (wall clock time of 38873 s, or 10.8 hrs). The computational efficiency of the model was found to be highly dependent on the mesh size. Furthermore, the running time increased exponentially with seed size. As such, the 4 mm seed size was chosen based on the benefit of allowing multiple analyses to be run in relation to the time constraints of the present study.

It should be noted that the difference of results, especially during load application, are significant between models of varying seed sizes and such the results of the present study will be treated with this in mind. A mesh sensitivity analysis has not been conducted for the soft tissue components of the model as the author has already investigated this in a previous study (McLennan & Pankaj, 2016). Here it was found that using a 1 mm seed size for cartilage and menisci parts produced results in accordance with clinical observations. Furthermore, the fineness of 1mm elements produces an appropriate number of 'element layers' through the soft tissue depth so as to produce an adequately extensive distribution of stresses and strains through the soft tissue depth.

Table 4.1 Model sizes and running time of the 3D knee joint model for different mesh coarseness of the bone parts.

Seed Size (mm)	No. of Truss Elements	No. of Shell Elements	Central Processing Unit (CPU) Time (s)
4	103594	7480	6491.5
3	198819	10550	10471
2	1349779	29272	89078

The complete modelling process is illustrated in the flowchart below:
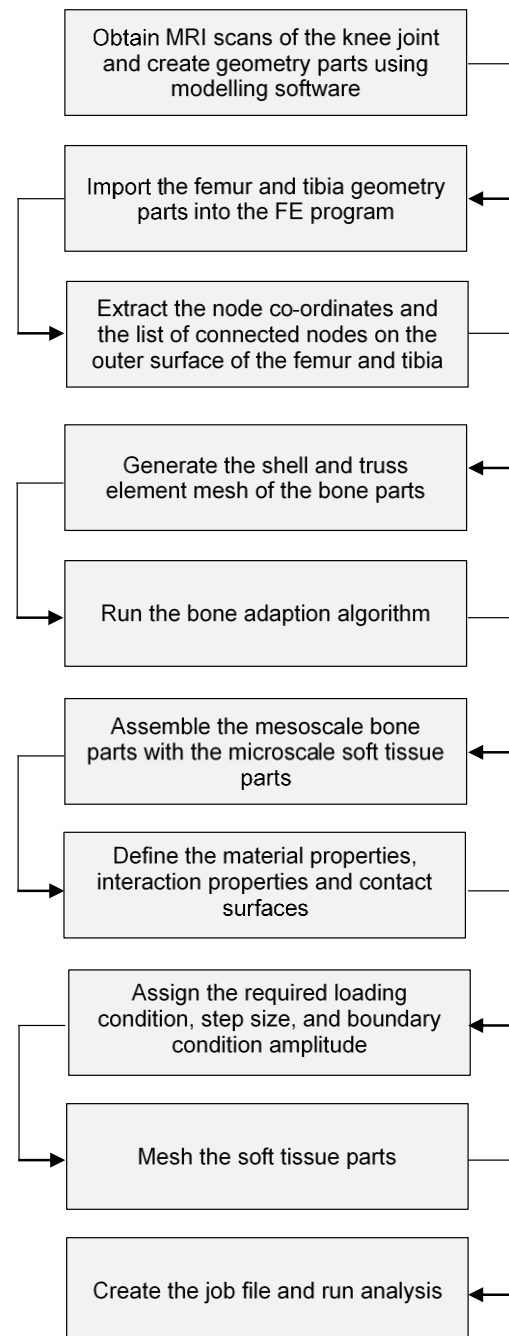
4.5 Validity of the Bone Generation Method for Finite Element Analysis

4.5.1 Validity of the Bone Model Parts
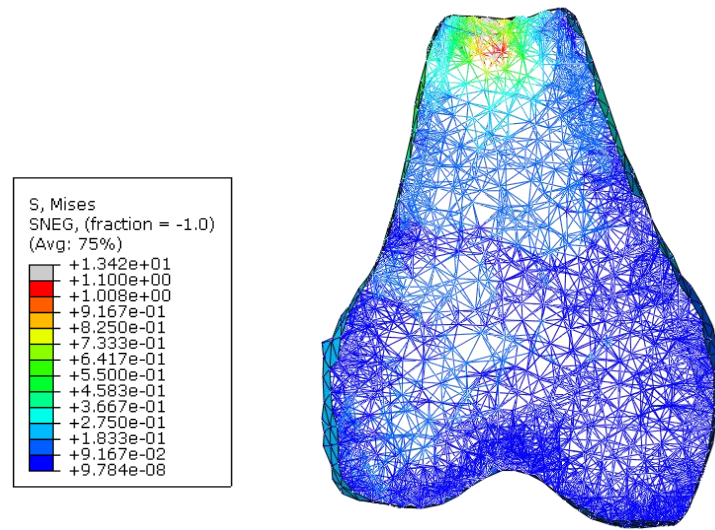
Figure 4.8 Frontal plane 5 mm slice of the VMS stress state within the femur part of the FE model at the end of the one-hour loading scenario.

Figure 4.8 conveys the greater stresses in the inner truss elements compared to the outer shell elements of the femur. This is due to the slender strut-like nature of the truss members which carry the load axially resulting in smaller cross-sectional areas relative to the shell elements. In turn, this results in greater stresses. The shell elements carry load via a combination of loading actions such as axial resistance, membrane resistance and bending. This accounts for the harder cortical bone on the outside of the femur and the sponge-like inner trabecular bone.

A notable stress concentration was observed at the top of the bone part due to the point of load application being at a single node. A more realistic study could take advantage of applying a pressure load over the top surface of the femur part or applying multiple concentrated loads at different nodes in order to better distribute the applied load.

4.5.2 Validity of the Soft Tissue Model Parts
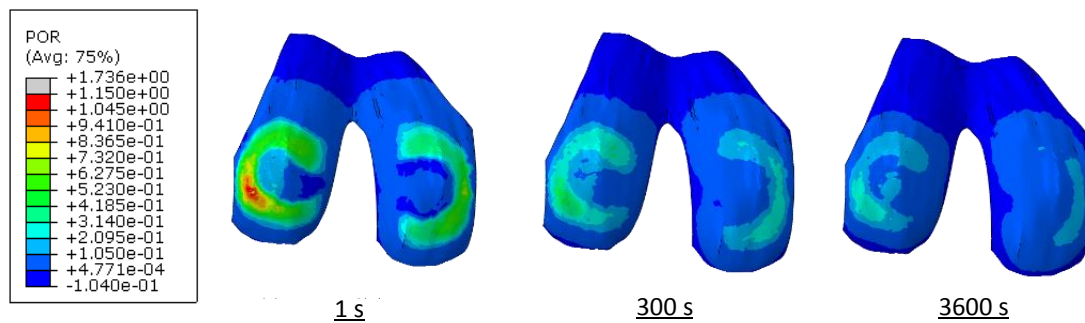
Figure 4.9 Pore pressure response on the superficial surface of the femoral cartilage throughout the analysis. Left to right: 1 second, 5 minutes and one hour. Note: these contours plots were taken from the OA indicative model.

In addition to the study of the femur mechanical response, the biphasic mechanical response of the cartilage was also studied. The change in pore pressure at the superficial surface of the femoral cartilage is displayed in Fig. 4.9. Immediately after full application of the load, the pressure was observed to concentrate through the depth of the cartilage at the menisci contact areas on both the medial and lateral sides, reaching a maximum value of 1.15 MPa. Gradually, the pressure reduced as the pore fluid escaped the soft tissue components and the solid phase took over the load carrying responsibility. The minimum pressure was found to be 0.21 MPa at the end of the one-hour loading condition.

The rate of decrease in the pore pressure slowed towards the end of the analysis suggesting that the knee joint system was reaching a state of equilibrium. In damaged soft tissue components, increased permeability is often observed. This was implemented into the model and the results analysed (Fig. 4.9). The pore pressure was found to decrease faster throughout the simulation with the solid phase playing a greate role in load carrying as a result. This suggests that additional stress may arise on the solid constituents of the articular cartilage ECM in OA patients.
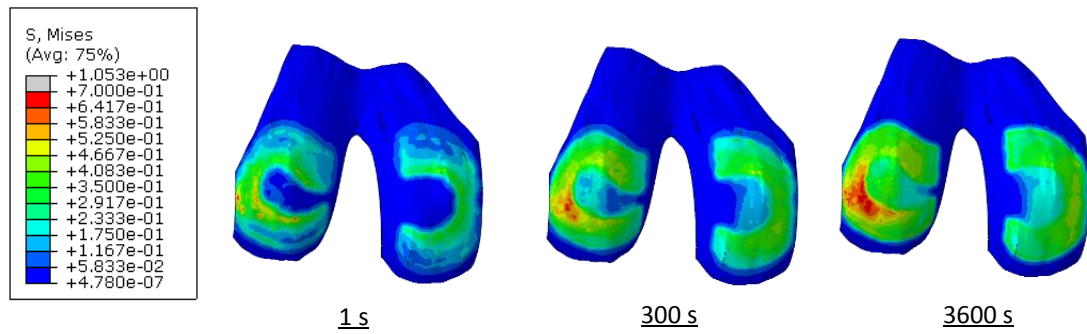
Figure 4.10 VMS response on the superficial surface of the femoral cartilage throughout the analysis. Left to right: 1 second, 5 minutes and one hour. Note: these contours plots were taken from the OA indicative model.

Similarly to the pore pressure response, the menisci contact areas on the femoral cartilage experience the greatest stress of the solid phase (Fig. 4.10). As fluid continues to escape, the cartilage compresses to the point where the femoral cartilage makes contact with the tibial cartilage, this produces a central stress response on both the medial and lateral sides of both the femoral and tibial compartments of the cartilage. As the step time increases the stress concentrations expand outwards covering more of the cartilage area. This implies that during extended bodyweight loading, a larger area of the cartilage experiences growing stresses. Additionally, the initial stress concentration towards the central cartilage areas may highlight areas most prone to repetitive loading damage and in turn the areas in which OA propagates from.

4.5 Osteoarthritis Pathways

4.5.1 Areas of Stress Concentration on the Cortical Bone of the Femur
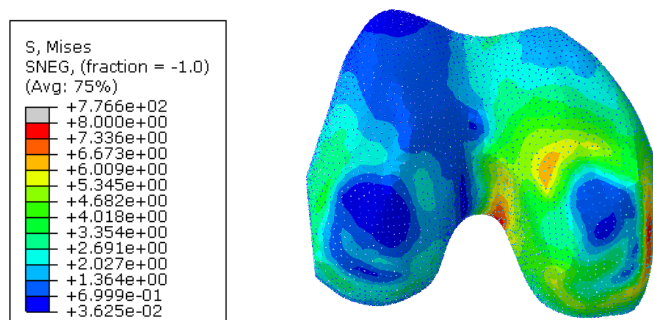
Figure 4.11 VMS contour plot on the lateral condyle (left) and medial condyle (right) of the femur. Note: the contour plot is of the healthy model.

From analysing the healthy model, it was found that the shell elements experience a relatively uniform stress distribution (Fig. 4.11). The greatest stress occurred on the outer side of the medial condyle where a VMS of 8 MPa was reached. This stress concentration coincided with the axial alignment of the menisci parts which was expected as this is the main path of load transfer during fully extended bodyweight loading.

Of the two condyles, the medial condyle experienced the greater VMS response throughout the analysis, however, this most likely differs between patients which limits the conclusions that can be drawn from the observation. With that said, changes in stress distribution on the two condyles may result from bone degradation. It follows that if clinical observations can be made of the stress distribution across the two condyles in knee joints indicative of OA, FE models can then be used to determine mechanical causes of such distributions by trying to replicate the findings using a variety of biomechanical set-ups, i.e. a distinct region of bone or soft tissue may be causing excessive stress in a certain area and as such that distinct region should be treated to mitigate the excessive stress.
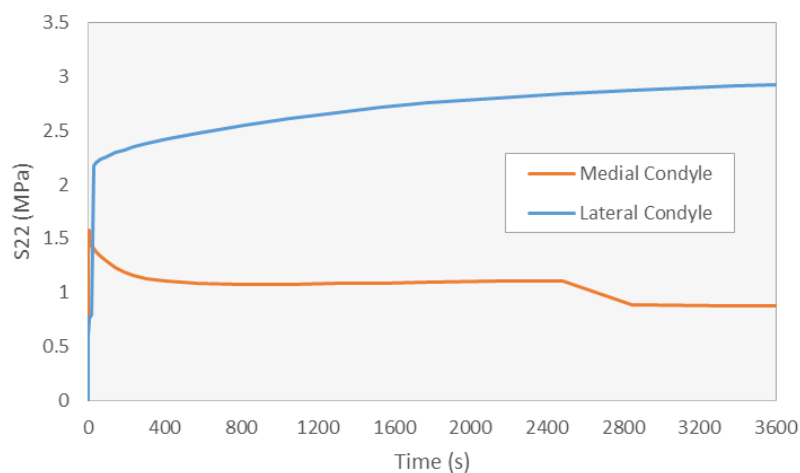
Figure 4.12 Comparison plot of the maximum nodal axial stresses on the medial and lateral condyles of the femur. Note: the selected nodes were situated on the femur-to-femoral cartilage interface surface.

The stress state in the two condyles was found to remain similar upon application of the load, however, the same cannot be said for the soft tissue components. This is a result of the poroelastic material properties of the cartilage and menisci taking a longer time to reach mechanical equilibrium between the fluid and solid phases, where conversely the bone simply has a single solid phase.

Figure 4.12 shows the variation in the vertical stress response at one node on the medial condyle of the femur and another on the lateral condyle of the femur. Interestingly, this differs from the VMS findings which showed the reverse. A possible explanation for this could be the bone adaption algorithm generating thinner shell elements on the lateral side, due to the algorithm recognising the area as being less crucial in load carrying, resulting in greater stress values.

It should be noted that bone may also be modelled as poroelastic to represent the bone fluid, however, this was not done in the present study as the pore fluid of the soft tissue components has a greater importance in terms of the mechanical response of the joint when compared to that of the bone.

4.5.2 Comparison to the Simplified Geometry Model
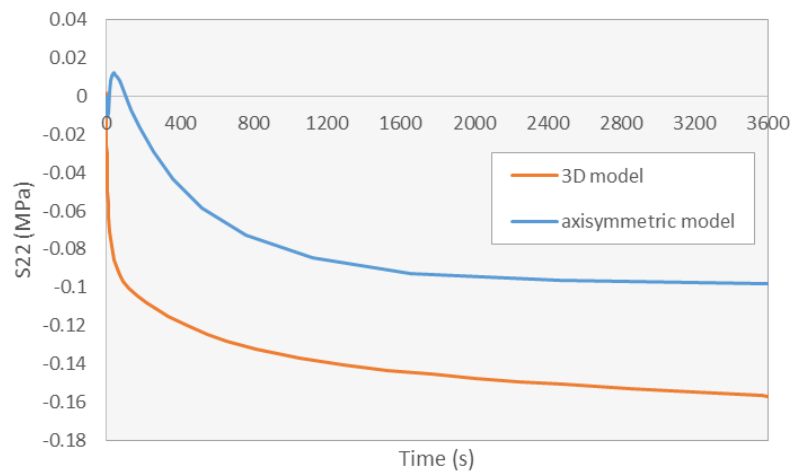
Figure 4.13 Comparison between the axial stresses of the simplified and 3D model. Values were taken from the central position of the soft tissue parts (medial side of the femoral cartilage for the 3D model) at mid-depth.

To assess the validity of the simplified geometry model for modelling knee joint biomechanics, the axial stress response at the centre of the axisymmetric cartilage part was compared against that of the centre of the 3D complex geometry cartilage part. It is shown in Fig. 4.13 that the simplified model slightly underestimates the stress response within the cartilage by an approximate magnitude of 0.04 MPa. Despite the degree of difference, this was deemed to be a relatively close correlation as the axisymmetric model contained several idealisations such as simplified bone and cartilage geometry along with simplified fluid escape surfaces which diverge it from the 3D model.

It follows that the simplified geometry model may be appropriate in studies where computational efficiency is important, however, with the trend of study into bone-cartilage OA progression it is more appropriate to characteristically model the full geometry to develop a better understanding of the disease pathways. In addition, FE software is becoming ever more advanced because of computational advancements meaning the numerical data constraints of large 3D models are no longer as restraining as they once were.

Another possible cause of the lower stress in the simplified model is the uniform pressure distribution assumption over the bone and soft tissue. As shown in the previous sections of this chapter, the 3D model has a non-uniform distribution of pressure of the cartilage surface which may result in greater stress responses. The 3D model experiences a greater stress as the simplified model assumes a uniform distribution of pressure when the actual shape of the femur condyles concentrates the load towards the stiffer central regions of the soft tissue compartments.
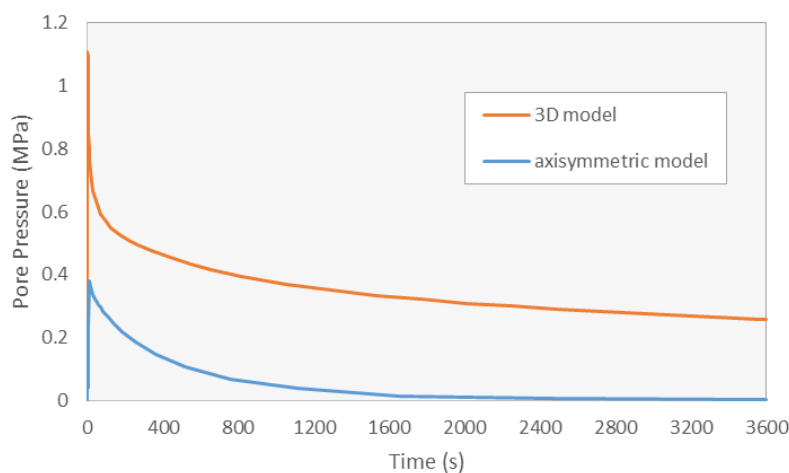
Figure 4.14 Comparison between the pore pressure responses of the simplified and 3D model. Values were taken from the central position of the soft tissue pieces (medial side of the femoral cartilage for the 3D model) at mid depth.

The smaller value of pore pressure for the simplified geometry model (Fig. 4.14) throughout analysis was most likely due to the less realistic escape surfaces of the simplified model. These escape surfaces are deemed oversized when compared to the actual soft tissue escape surface arrangement. Despite the average difference in magnitude of 0.4 MPa, the similar shape of response over time for both models validates the use of the simplified geometry model as modifications can be made to the boundary and loading conditions in order to create better correlation with the results of the more realistic model.
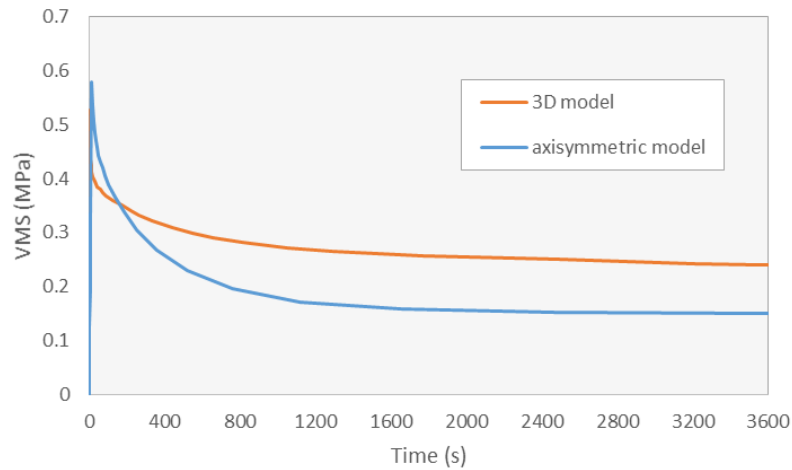
Figure 4.15 Comparison between the VMS response of the simplified and 3D models. Values were taken from the central position of the femur-cartilage interface (medial condyle of the femur for the 3D model).

A good correlation is seen between the VMS responses at the bone-cartilage interface of the two models. A relatively small increase in initial stress of 0.34 MPa is observed for the simplified geometry model (Fig. 4.15). Again, this is possibly due to the more representative geometry of soft tissue components in the 3D model leading to thicker cartilage parts when compared to the uniform 2 mm depth defined in the simplified geometry model. Due to the thicker cartilage, pore fluid escapes at a slower rate due to the longer escape path. From this, the pore fluid carries more of the initial load in the 3D cartilage as the fluid is yet to dissipate which in turns leads to smaller solid phase stresses and strains.

Both models can be seen to tend towards similar values under the same loading, hence, the simplified geometry model may be more applicable when long term mechanical response of the knee joint is to be studied.

4.5.3 Comparison of the Healthy and Damaged Models

To better understand the mechanical consequences of OA damage, an 'OA indicative' model was produced and analysed. It has been established that bone mass density decreases with age at rates up to 10.2 mg/cm^(2) for osteoporotic patients (Kado et al., 2000) To do so, the stiffness properties of soft tissue in the healthy model were reduced by a value of 12% obtained from Obeid, Adams & Newman (1994), while the permeability was increased by a value of 48% obtained from Mow et al. (1994).

Older bone shows more brittle behaviour due to collagen changes (Keaveny, Morgan & Yeh, 2003). This can be modelled by reducing the stiffness value, in the case of the present study, the stiffness was simply reduced by a third of its value in the healthy model to 12 GPa. Hansen et al. (2008) found the reduced stiffness value of moderately damaged bone to be 17 GPa by taking the average of the compressive and tensile stiffness values of a bone specimen, however, the OA indicative stiffness of the present study was reduced further to represent severe OA. Additionally, the number of truss elements per node was reduced from 16 to 8 so to model the degradation of the trabecular bone (the radius of the truss elements was limited to prevent the bone adaption algorithm over compensating for the reduced number of connections) (Fig. 4.16). It should be noted that this method of modelling bone degradation was very much intuitive and was only considered acceptable as this study seeks to form a basis for future models that will have the benefit of more accurate clinical data of OA effects.
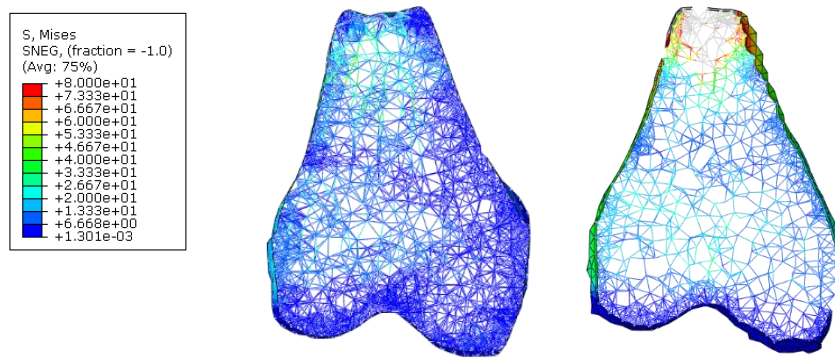
Figure 4.16 5mm slice VMS plots of the femur after one-hour of bodyweight loading. LHS: Healthy model. RHS: OA model.

Figure 4.16 conveys the more severe stress response in the damaged femur model part. As stated previously, this results from the reduced number of truss elements meaning the remaining truss elements must carry more of the bodyweight. This forms an insight into the amplification loop-like effect of OA damage where the remaining elements experiencing greater stresses are more likely to fail, leading to ever increasing stresses in the remaining elements. By modelling the areas of degradation, it is hoped that this study can aid clinical treatments by helping to best identify areas susceptible to the development of bone damage.

By increasing the soft tissue permeability, the damping effect of the cartilage and menisci on the femur was found to reduce which resulted in a more sudden stress increase to the femur which in turn resulted in further damage to the bone. Again this provides useful insight into OA development.
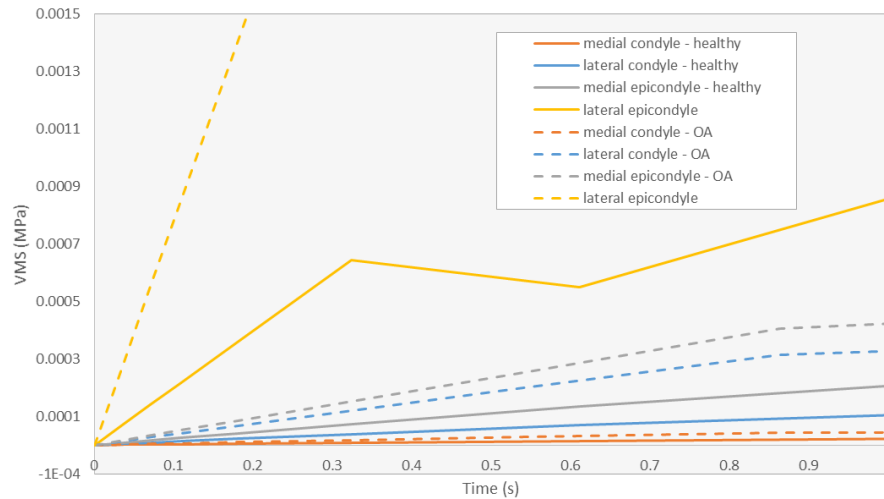
Figure 4.17 Comparison of VMS response during application of bodyweight load to the knee joint, measured at corresponding points of the healthy and OA FE models. Note: the unbroken lines represent the healthy model while the broken lines represent the OA model.

The VMS response of the OA model in comparison to the healthy model was found to be greater on the lateral condyle and epicondyle, but smaller on the medial condyle and epicondyle (Fig. 4.17). The most notable difference occurred at the medial condyle node location where the OA model experienced an increase in stress of 4.1 MPa from the stress in the same location on the healthy model. The increase in stresses at the medial locations suggests that this particular location may be more prone to mechanical damage.

One caveat of this observation is that the response of the bone is dependent of the subject geometry. It, therefore, follows that to draw useful conclusions, one must analyse multiple subject-specific geometries to establish if the lateral epicondyle is a recurring 'problem' spot within damaged knee joints.
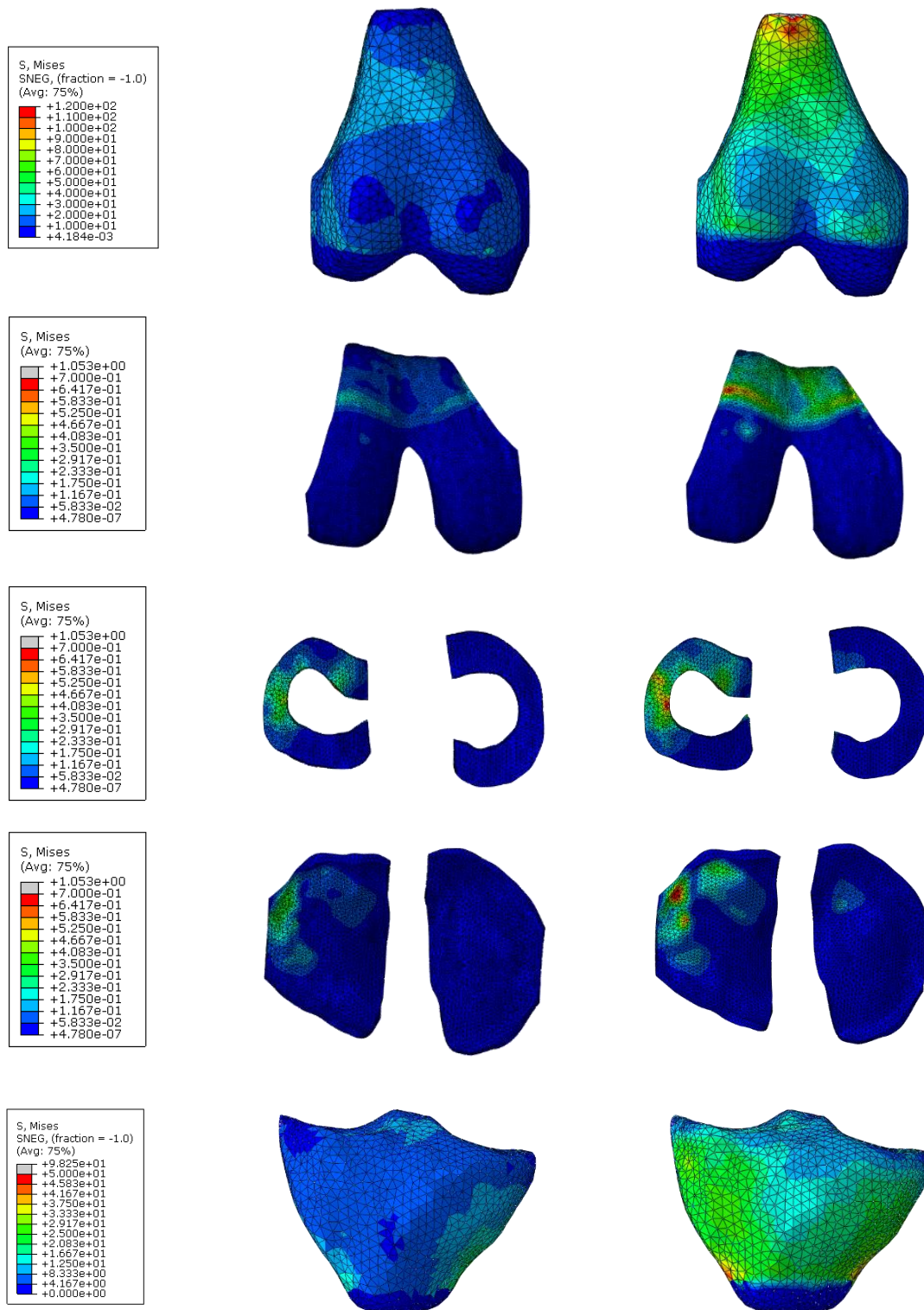
Figure 4.18 Exploded isometric visualisation of the healthy (LHS) and OA (RHS) models, showing the VMS distribution on each component of the knee joint. Note: the shown values occur after one hour of bodyweight loading.
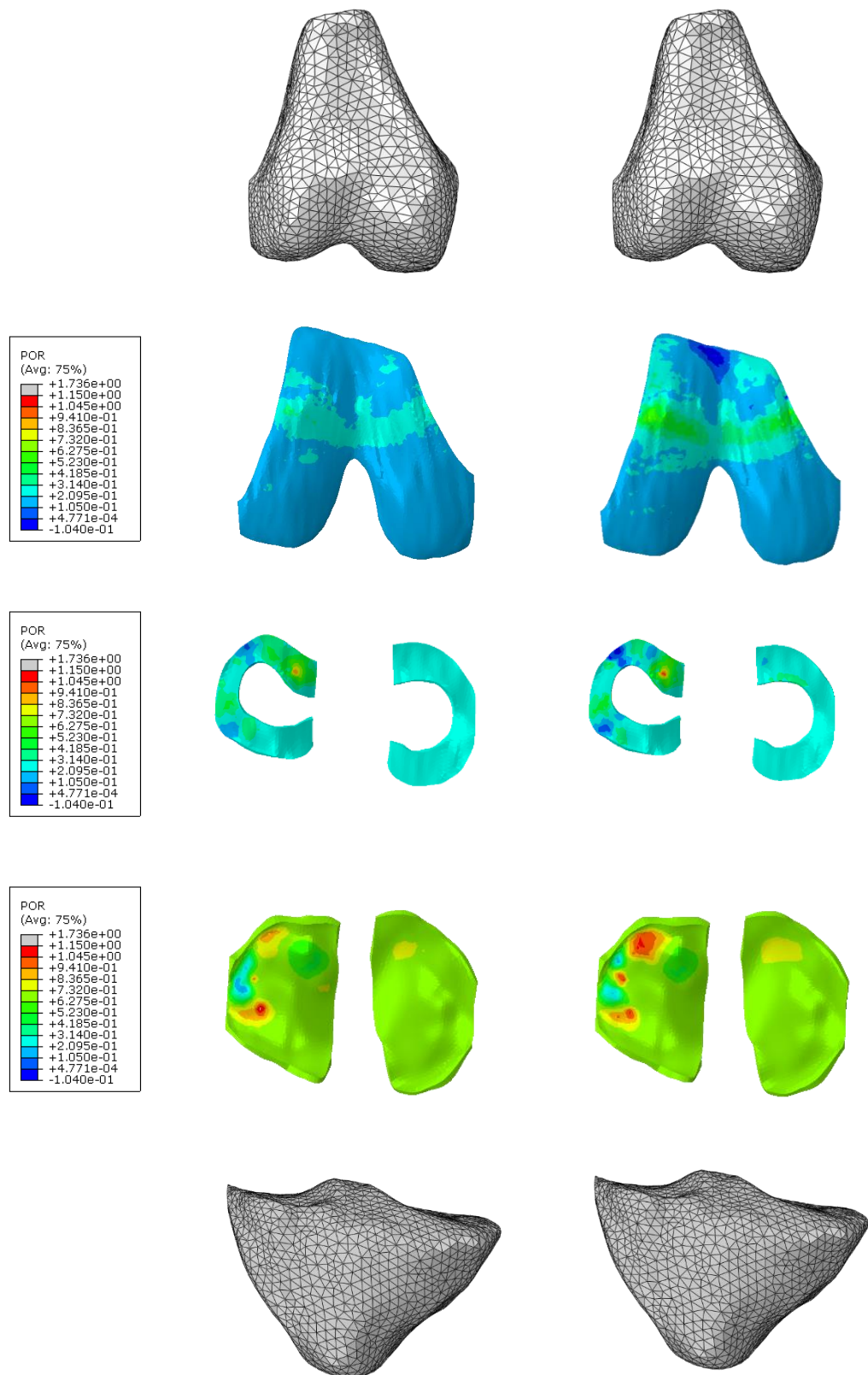
Figure 4.19 Exploded isometric visualisation of the healthy (LHS) and OA (RHS) models, showing the pore pressure distribution on each component of the knee joint. Note: the shown values occur immediately after full application of the load.

Figure 4.18 provides a schematic representation of the VMS response across all the mechanical components of the knee joint model for the healthy and OA cases. The values were taken after 3600 s of bodyweight loading. Very low stresses were observed at the femur-articular cartilage interface relative to the stresses observed on the outer shell elements of the upper femur. A possible cause of this may be the damping-like effect of the cartilage immediately below the bone. As the concentrated load is applied over one hour, the cartilage and menisci act together as a 'softening sponge' to the femur that has a decreasing damping effect throughout the analysis as an increasing amount of pore fluid has escaped. Despite the decreasing damping effect with time, the softening action was found to be present throughout the entire analysis hence resulting in the smaller stress build-up of the femur-articular cartilage interface.

The average VMS in the OA model were observed to be approximately 1×10^{-5} MPa greater than that in the healthy model during the main constant load phase of the analysis. The reasons for this are the same as those discussed for the simplified model (see Chapter 3). Notably, the soft tissue experienced greater stress on the lateral side. The maximum VMS differences between the two models on the soft tissue component surfaces were as follows; femoral cartilage 0.55 MPa, menisci 0.32 MPa and tibial cartilage 0.36 MPa. For both the femur and tibia cortical bone, the approximated VMS stress increase was found to be 50% when applying OA indicative properties to the model. This is greater than the 30% approximated average stress increase for the trabecular bone (Fig. 4.16).

Figure 4.19 shows the pore pressure response of the cartilage and menisci. The shown visualisations were taken at 1 s into the analysis which corresponds with the initial point of full load application and as such the point at which the soft tissue experiences the greatest pore pressure (as the model runs beyond 1 s, the pore fluid dissipates causing the pore pressure to drop). Analysis of both the models showed the pore pressure to be approximately 0.11 MPa greater in the OA model. This conflicts with the findings of the simplified geometry model. This is most likely due to the combination of altered bone parts causing a faster rate of compression over the soft tissue parts and decreased solid phase stiffness of the cartilage and menisci. Much like the VMS distribution pore pressure concentrates towards the lateral side of the joint.
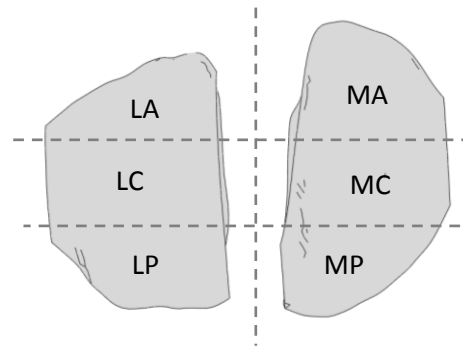
Figure 4.20 Schematic of tibial articular cartilage regions. MA - medial anterior, MC - medial central, MP - medial posterior, LA - lateral anterior, LC - lateral central and LP - lateral posterior.
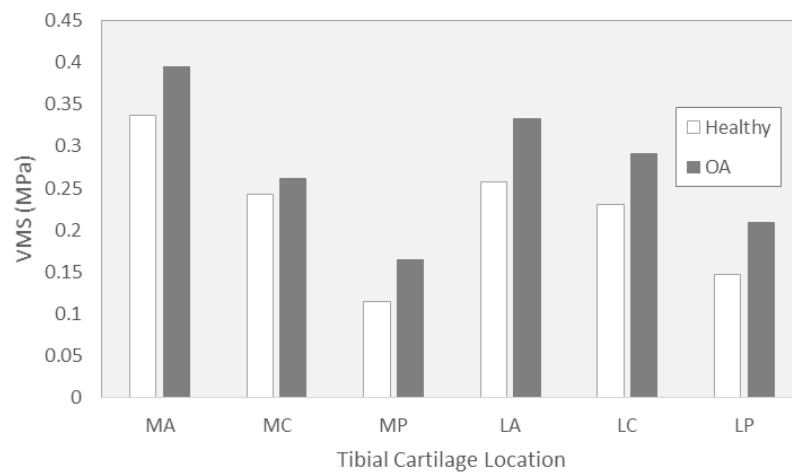
Figure 4.21 Comparison of the different VMS values on the superficial surface of the tibial cartilage between the healthy and OA models. Note: the values have been taken at 3600 s.

Figure 4.20 shows the different regions on the superficial surface of the tibial cartilage that were investigated. The variation in VMS across the tibial cartilage superficial surface is graphically illustrated in Fig. 4.21. At all selected points, the OA model experiences higher stress under the same load case. The greatest difference was found in the lateral anterior region where the difference between the severe OA model and the healthy model was found to be 0.07 MPa. Although the difference is relatively small, the result suggests that this region may be more prone to progressive damage from excessive stress after the onset of OA. Again, it is important to note this finding is specific to the patient-geometry used in this investigation. To draw strong conclusions, one must find the lateral anterior region to be patient-specific in multiple patient-geometries.

4.6 Discussion

4.6.1 Suitability of Combining mesoscale and microscale Parts within a Single Model

In the analysis of the truss element distribution in the 5 mm femur slice, it was noted that the medial and lateral locations showed a denser concentration of trabecular bone elements when compared to clinical images. A possible cause of this is over-compensation by the bone adaption algorithm due to the exclusion of ligament and muscle forces in the model. The ligament and muscle forces provide stability to the joint which alleviates the need for additional trabecular bone in the medial and lateral areas of the femur.

4.6.2 Limitations

The limitations of the multiscale model as presented in this study are as follows:

- The point load, located at the upper surface of the femur segment, does not entirely represent the true spread of the load across the femur cross section. As such, higher than wanted stress concentration occurs at the point of load application and the spread of load transfer across the femur-femoral cartilage interface will vary from the *in vivo* scenario. For a complex, non-uniform cross-section such of that of the femur it is difficult to apply a pressure load, however, this can be adequately represented using an idealised assignment of load applicators and inertia applicators via a series of carefully chosen point loads (Villette, 2016).
- Results are specific to the single patient geometry used to create the model. Therefore, generalised research conclusions should be treated with caution as they may not apply to all OA patients.
- The ligament effect and muscle forces were idealised by using fixed supports on the nodes on the bottom face of the tibia part. This ignores the effects of the bone, muscles and ligaments below the location of the fixed base and as such limits the type of loading conditions that can be simulated using the model.
- The musculoskeletal (MSK) approach requires consideration of the entire bone system to accurately model knee joint behaviour. For example, an indirectly related bone, elsewhere in the body from the knee joint, can act as a lever arm under a different load condition which can cause significant difference in the load paths through the knee joint. This effect was not considered in the present study.

4.7 Conclusions

The main conclusions drawn from this chapter of the study are as follows:

- The bone adaption algorithm presented in this chapter provides a relatively good approximation of the trabecular and cortical bone distribution within the femur and tibia.
- The bone adaption algorithm is effective at generating the bone type distribution for a variety of everyday loading conditions and can be used to predict bone type distribution indicative of OA damage to the bone associated with the knee joint.
- The bone adaption algorithm can be improved by simulating the ligament and muscle force effects that act on the knee joint. As mentioned, without these considerations the algorithm unwantedly compensates by producing both an excess number and excess size of the truss elements.
- Multiscale models are less computationally expensive than total microscale models while being more realistic than entirely macroscale models.
- The results presented are dependent on patient-specific geometry and as such, future studies would be wise to study an appropriate number of patient-specific geometries before drawing general conclusions.
- The mechanical response of the knee joint under bodyweight loading using the presented FE model is more realistic when applying a pressure load opposed to a nodal point load.
- Due to the limitations of present software, modelling of depth-dependent properties in the soft tissue components proves difficult and to do so one may find more success using a simplified geometry model such as the one presented in Chapter 3. It is hoped this complication will be mitigated by future advancements in FE analysis software.
- The VMS and pore pressure response of the respective joint components of the multiscale model compare well to those of the simplified geometry model. The findings also agree with those of previous studies highlighting the benefits of using multiscale modelling techniques.
- By comparing the healthy multiscale model with the damaged, severe OA indicative, multiscale model, it was found that disease-initiated changes in the joint lead to changes in stress distribution and magnitude in the bone and soft tissue components of the model.

CHAPTER 5 ROTATIONAL AND GAIT ANALYSIS OF THE MULTISCALE FINITE ELEMENT THREE-DIMENSIONAL KNEE JOINT MODEL

5.1 Rotational Analysis

5.1.1 Introduction

Observed knee joint misalignment is a strong predictor of OA in terms of both the development and progression of the disease (Petersson & Jacobsson, 2002). High tibial osteotomy (HTO) is a clinical treatment used for treating joint misalignment in mild to moderate OA patients. The procedure involves making a cut in the tibia such that the head of the tibia can be re-aligned with the goal of regaining joint health. The procedure is less commonly used now given the success of full knee joint replacements, however, as the procedure does not violate the joint itself, it is still often used when a non-invasive procedure is required.

To further develop and investigate the effectiveness of the multiscale model presented in the previous chapter, the effects of misalignment and HTO on the mechanical behaviour of the knee joint have been investigated. The misalignment was simulated using an applied varus moment to represent the distal segment of the knee joint pointing inward. As such, the ligament geometry parts were now added into the model of the previous chapter to better simulate the mechanical response of the joint.

Prior research of knee joint misalignment has been carried out (Andriacchi et al., 2000), however, research utilising a multiscale model is, at present, limited. This section of the dissertation seeks to partially fill this gap in the literature and to provide the framework for future investigation.

5.1.2 Modelling Method

The majority of the modelling methodology was the same as presented in Chapter 4. The deviations from the modelling method of Chapter 4 are as follows:

- Associated ligament parts of the knee joint were included. These were meshed using 4-noded linear tetrahedron elements (C3D4) with a seed size of 1 mm (Fig. 5.1). This seed size was based on the study by Mootanah et al. (2014) where a similar computational model of the same seed size and were was used while maintaining an error of less than 5 % throughout analysis compared to a reference model.
- The ligaments were attached to the respective bone parts using tie constraints with node-to-surface contact.
- The step time was 1 s, with the moment and concentrated force loads being applied linearly over this time.
- The bodyweight load was set to 374 N and the varus bending moment to 15 Nm about the vertical axis. Again, this was based on the study by Mootanah et al. (2014).
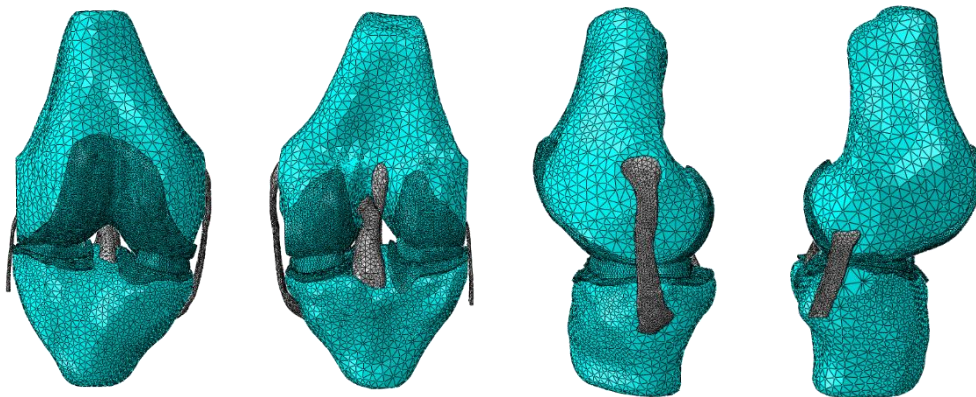
Figure 5.1 Composition of ligaments within the multiscale FE 3D model. Note: the ligaments are shown in grey and have been modelled as microscale. From left to right: anterior, posterior, medial and lateral elevation view.

The Young's modulus values of the ligaments were linearly increased during the analysis to better represent the in vivo knee joint scenario. These initial Young's moduli values were as follows; medial cruciate ligament (MCL) = 10 MPa, lateral cruciate ligament (LCL) = 60 MPa, anterior cruciate ligament (ACL) = 250 MPa and the posterior cruciate ligament (PCL) = 40 MPa (Mootanah et al., 2014).

The Neo-Hookean coefficients (D1 and C10) and the shear (μ_0) and bulk (k0) moduli throughout the analysis were obtained using Eq. 5.1 to 5.4 by substituting in the linear increments of the Young's moduli.

$$K_0 = \frac{E}{3 \times (1 - 2 \times \nu)}, \qquad (5.1)$$

$$\mu_0 = \frac{E}{2 \times (1 + \nu)}. \qquad (5.2)$$

$$D_1 = \frac{2}{K_0}, \qquad (5.3)$$

$$C_{10} = \frac{\mu_0}{2}. \qquad (5.4)$$

5.1.3 Results and Analysis
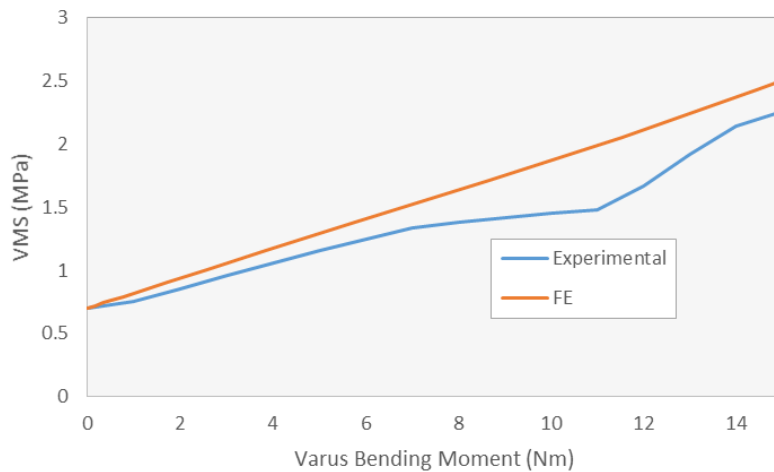
Figure 5.2 Tibial cartilage medial compartment VMS response comparison of experimental data and the FE 3D ligament-inclusive model. Note: the experimental data was taken from Mootanah et al. (2014). A 374N axial load plus a 15Nm varus bending moment was applied to both the clinical specimen and computational model.

It can be seen in Fig. 5.2 that the VMS response in medial tibial cartilage with respect to the increase in misalignment, shown as bending moment, correlates well with that of the clinical specimen in terms of both shape and magnitude. However, slight variation can be seen between 8 Nm and 14 Nm loading points. This is most likely due to the FE modelling assumptions such as restriction of the femur DOFs producing smoothing of results.

The experimental test used the same loading and boundary conditions as the FE model of the present study.

5.1.4 Discussion

It should be noted that none of the mentioned prior studies used poroelastic materials. This could be a possible cause of the noted variation between experimental and computational values. In addition to the inclusion of poroelastic elements, future studies may also wish to elaborate on the effect that misalignment has on the distribution of stress between the medial and lateral sides of the bone and soft tissue within the knee joint.

The occurrence of changes in stress distribution was highlighted by Tetsworth & Paley (1994) who found that a 5 ° increase in varus misalignment leads to an increase of medial compressive loading from 70% to 90%. Furthermore, Mootanah et al. (2014) found that increasing the varus bending moment from 4 Nm to 8 Nm resulted in an increase of medial compartmental force percentage of 73% to 89%. Neither of these studies included multiscale modelling or poroelastic soft tissue properties, as was done in the present study, hence there is scope to further this line of research.

5.2 Gait Cycle Analysis

5.2.1 Introduction

To further investigate the multiscale FE model's ability to simulate OA patient loading patterns, a gait cycle analysis was conducted. This involved simulating a ten-step level-walking barefoot loading cycle of a person of average weight. The results were then analysed to see which of the two tibial cartilage compartments carries the greater axial strain and to establish the regional variation in terms of maximum axial strain. The results were then validated against previous studies to assess the appropriateness of using a multiscale model for investigating the biomechanical response of the entire knee joint.

5.2.2 Modelling Method

Table 5.1 Patient-specific level-walking barefoot data. Taken from the OrhtoLoad Database. Note: the shown values correspond to an elderly female patient with a bodyweight load of 814 N.

OrthoLoad Data - BW = 814.0N		
Direction	Max. Force	Max. Moment
	(%BW)	(%BWm)
x	-13	2.34
y	-21	2.05
z	-318	0.91
Magnitude	319	2.42

Again, idealisations of the actual mechanical scenario were made to achieve computational efficiency. The axial load of three times that of the original bodyweight was represented using a 1.5 mm displacement of the femur part. In other words, this simulated the impact loading that arises through the knee joint during a walking cycle. This assumption was based on clinical data (OrthoLoad, 2015) where the maximum axial force in the knee joint during walking was found to be 318% of the level-standing bodyweight (Tab. 5.1).
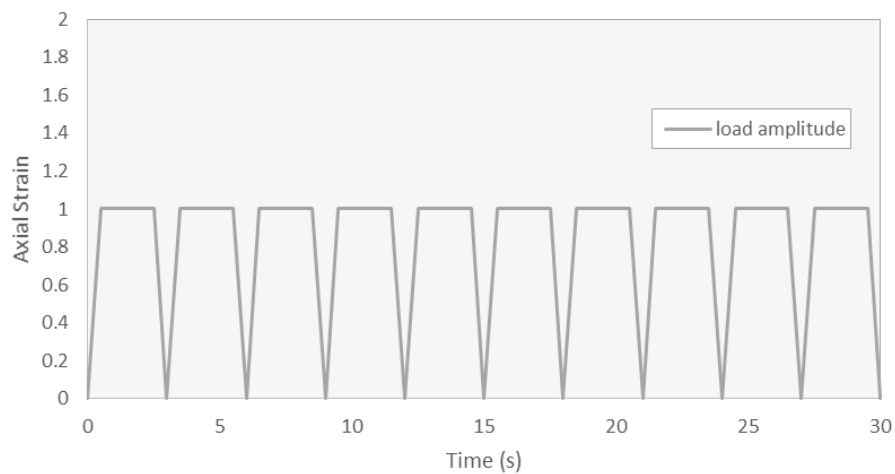
Figure 5.3 Gait amplitude for a 30 s (ten-step) loading cycle.

To simulate the cyclic loading pattern, an amplitude was assigned to the load (Fig. 5.3). This amplitude represents the weight bearing of each leg during a ten-step gait cycle where the load is fully applied over a period of 0.5 s, then held for 2 s and removed over a period of 0.5 s.

A more realistic load amplitude would take a less uniform and more sinusoidal-like form such as the ones found in the OrthoLoad database, however, the present study only seeks to validate the knee joint model for basic loading scenarios and hence a detailed gait loading assignment was deemed unnecessary. With that said, future studies that seek to fully understand the response of the knee joint during gait cycles should keep in mind the approach of the present study is an idealisation of the true scenario.

5.2.3 Results and Analysis
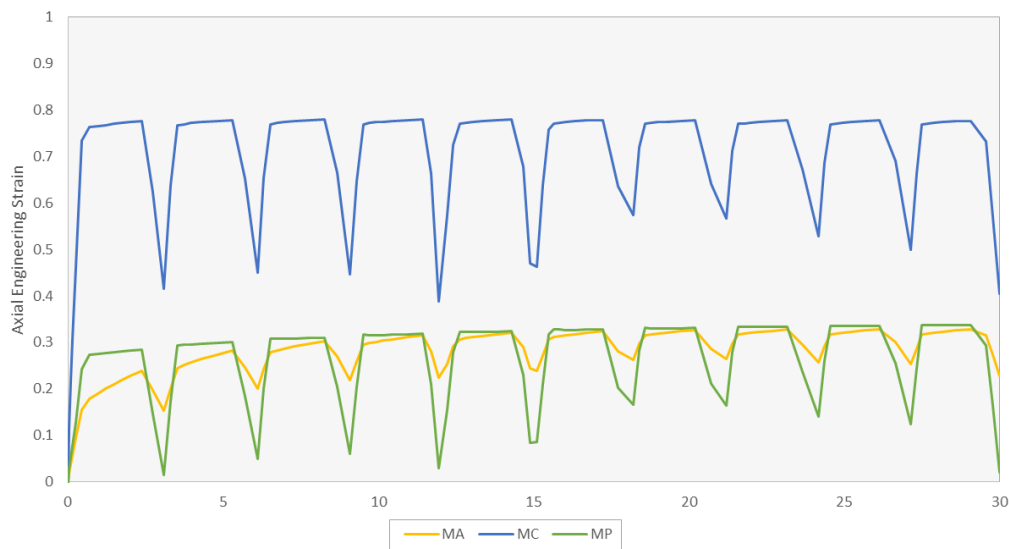
Figure 5.4 Axial strain response across the medial tibial cartilage during a level-walking gait cycle.
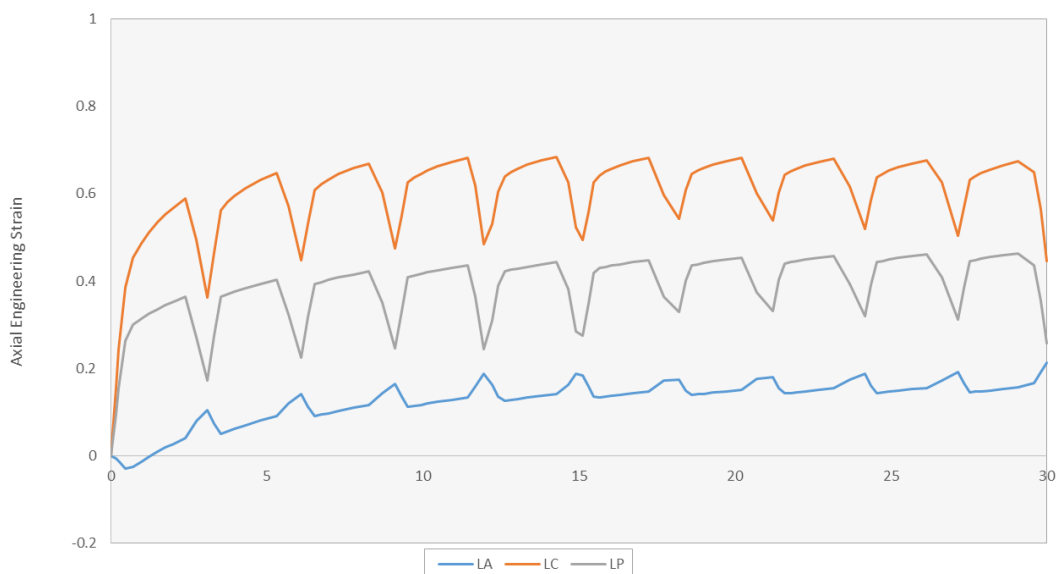
Figure 5.5 Axial strain response across the lateral tibial cartilage during a level-walking gait cycle.

Figure 5.4 and 5.5 display the different axial strain responses across the medial and lateral tibial cartilage compartments, respectively. The central region of the medial compartment experiences greater strain throughout the analysis compared to the central region of the lateral compartment. The critical strain region, the medial central region, experiences an average axial strain 11.0% greater than the comparative lateral central region.

With each step cycle, the peak axial strain is seen to increase. The probable cause of this is a cumulative strain response due to the sponge-like effect of the cartilage. As the load is applied the cartilage compresses as pore fluid is released at the escape surfaces. With each step cycle, the cartilage is compressed further, hence increasing the axial strain in the solid phase of the cartilage. In reality, pore fluid shall be re-absorbed as the load is removed which prevents damage caused by strain build up. The maximum axial strains were 78.0% and 68.4% in the medial and lateral compartments, respectively.

5.2.4 Discussion

As previously mentioned, the medial tibial cartilage compartment was found to experience greater strain compared to the lateral tibial cartilage compartment. This could indicate that the lateral compartment is more prone to OA damage, however, this finding is patient-specific and as such can only be used to aid clinical practice on an individual patient basis.

The finding of increased axial strain throughout the analysis compared well with a previous study by Saarakala et al. (2010) where the axial strain in the solid phase was also found to increase as the cartilage compressed during loading. Furthermore, the maximum axial strain values were comparable to a previous study of a similar nature (Lai & Levenston, 2010). Here the maximum strain was found to be 20% and 10% in the medial and lateral tibial cartilage compartments, respectively, when using a bodyweight load of 660 N. The present study found a similar ratio between the maximum strains of 32.8% and 21.3% in the medial and lateral tibial cartilage, respectively. The most likely cause for the difference of strain magnitudes between the two studies is the displacement-load assignment over-simulating the axial displacement of the femur part which results in greater soft tissue strains. Another contributing factor could be the significant differences in the geometry of the two models. It can be speculated that the lateral tibial cartilage is less active in terms of transmitting load in the model of the prior study.

The present study simply used the bone parts generated using the level-standing bodyweight bone generation based on the fact both the level-standing and gait simulations make use of an axial load applied to the same node along with the same material properties, meaning differences in the bone generation would most likely be negligible. Unfortunately, due to time constraints this was not investigated further, however, if future studies wish to also investigate the difference between the mechanical responses of bone for the two loading conditions, it would be wise to re-run the bone adaption algorithm using the gait-cycle loading for the successive adaption iterations as a precautionary check. Although differences are most likely small this would validate the assumption of the present study and, at the very least, produce a somewhat more representative shell and truss distribution for the femur and tibia segments.

CHAPTER 6 CONCLUSIONS

The main conclusions of the report are as follows:

- There is at present a gap in the literature regarding studies of multiscale models that combines all components of the knee joint. To fully understand the biomechanics of the joint without excessive computational demand, it is beneficial carry out research that makes use of multiscale models.

- Bone adaption modelling using shell and truss elements proves a useful tool for creating a realistic FE representation of the femur and tibia.

- To fully understand the mechanical response of the knee joint, specifically that of the soft tissue components, consideration of the collagen and PG network must be made within FE models.

- From analysing the simplified model, the stress within the soft tissue was found to be greater towards the outer surfaces, i.e. the zones closest to the pore fluid escape surfaces

- Furthermore, it was found by using the simplified model that after one hour of constant bodyweight loading the knee joint system is close to a state of mechanical equilibrium.

- FE studies into the knee joint are highly influenced by the geometry of the model parts and as such clinical research must make use of a wide range of patient-specific geometries when modelling OA development and treatment.

- The simplified model of the present study compares well against the 3D multiscale model and as such can act as a computationally efficient tool for studying the response on the knee joint in both healthy and damaged states.

- Depth-dependent properties prove difficult to model in 3D FE models due to limitations of the current software available to researchers, however, depth-dependent properties can be modelled in the simplified geometry model with relative ease.

- The multiscale model can be used for modelling OA pathways and progression under typical loading scenarios such as the presented prolonged bodyweight loading case.

- The multiscale model was shown to accurately model the mechanical effects of joint misalignment on the bone and soft tissue. Furthermore, the multiscale model can be used to model HTO treatment for OA patients and the arising consequences of such a procedure.

- Severe OA damage in both the bone and soft tissue of the knee joint, as shown using the multiscale model, leads to higher stresses in the tibial cartilage, possibly resulting in amplification of soft tissue degradation.

The findings from the all the presented models in this dissertation provide a number of applications for clinical care. These are as follows:

- By running a variety of loading simulations on both the simplified and multiscale model, the resulting findings can be used to influence and inform activity based rehabilitation programs for OA patients such as level-walking training for knee-joint transplant patients.
- With the increased study into 3D printed knee joint replacements, such as printable synthetic cartilage, the multiscale model can be used as a computationally efficient tool to analysis the response of the implants under a variety of load conditions. Another advantage of this is that the model removes the ethical concerns in studying the biomechanics of said transplants and can also highlight the interaction between the remaining biological bone and soft tissue and the newly implanted synthetic parts.
- The bone adaption algorithm can be modified to represent changes in bone growth and decay due to a variety of degenerative diseases. If, for example, clinical data suggests accumulated bone growth in a certain region due to mechanical alteration caused by OA, this can be readily implemented and considered in the adaption algorithm.
- Both the simplified and multiscale models can be used to inform clinical decisions by providing a convenient way to assess the effects of different treatment options on a knee joint model using patient-specific geometry and material properties.
- Aside from clinical application, the analysis of the current report can be validated and queried in future studies, providing a framework for future research endeavours.

CHAPTER 7 PROSPECTS OF FURTHER STUDY AND RESEARCH

Through the study of the existing literature and the analysis of both the simplified and 3D multiscale models, it was recognised that many important areas of research are yet to be conducted. These areas are highlighted in this chapter along with an explanation of how one may go about implementing them into future study.

Suggestions for future study include, but are not limited to, the following:

- To mitigate the errors arising from modelling assumptions, more realistic boundary conditions should be employed within the knee joint model. Furthermore, multiple loading conditions should be carried out to establish the variation and potential errors between each condition. This suggestion is based on the work of Speirs et al. (2007), who found that loading condition assignment has significant effect on mechanical fields, and also on the work of Phillips (2009) who established significant influence on bone models due to assumed boundary conditions.

- As previously mentioned, muscle forces and ligament action were not considered in the multiscale model. It has been suggested that incorporating wrapping surface constructs within the FE model leads to improved strain environment by simulating the compression and traction of muscle forces (Favre, Gerber & Snedeker, 2010). Furthermore, this will help avoid violation of the knee joint equilibrium condition.

- In place of idealising ligament and muscle forces for non-rotational analyses, future research may wish to include actual geometric representation of the ligaments. Bicer et al. (2010) found that the cruciate and collateral ligaments stabilise the knee joint and restrict rotations and translations of the femur with respect to the tibia. Conversely, or in addition, to the inclusion of ligament geometries, the role of the ligament can be simplified by restricting the movements of the femur (Pena et al., 2006).

- Phillips, Villette & Modenese (2015) found a 1.4% greater displacement when using truss elements for trabecular bone modelling compared to 2-noded Hermite-cubic Euler Bernoulli beam elements. This implies that the idealisation of structural architecture of the trabecular bone purely carrying load axially may not fully represent the *in vivo* mechanical behaviour. It follows beam elements that can additionally carry load in bending, may be more appropriate and as such, are recommended for future studies, where appropriate.

- The restricted range of truss radii and shell thicknesses can also be seen as a deviation from the true femur and tibia environment. It follows that a wider range of element sizes based on clinical observations should be included in future models (Treece et al., 2010).
- Further validation of results against experimental data would allow for more confidence in the results produced by the multiscale model.
- The present study only used the geometry and material properties of a single patient. A more conclusive study should use multiple patient-specific geometries and material properties to draw parallels and differences in the progression of OA throughout the knee joint. A more efficient way of achieving this would be to run many different patient-specific material properties within a single model of the same geometry each time.
- By using model material properties derived from literature in the present study, there is a certain degree of deviation from the true material properties of the original knee joint used to obtain the FE geometry parts. Shirazi, Shirazi-Adl & Hurtig (2008) established substantial influence on the knee joint contact mechanics when using different cartilage properties.
- A wider variety of everyday loading conditions should be included within future studies to fully understand both the mechanical response and development of OA damaged knee joints. This will better aid treatment for patients as a variety of situational tasks can be studied.
- In the multiscale model, the only time-dependent material property was the void ratios of the cartilage and menisci. To better the results, future studies should seek to include more time-dependent properties along with depth-dependent soft tissue properties such as stiffness increase towards the deep layers of the articular cartilage. While this was modelled in the simplified geometry model, it is difficult to do so when using complex 3D geometries. As such, future studies would be wise to establish novel ways of doing this.
- The ECM is known to change over time and during loading. A possible way of modelling this is to include collagen-fibril remodelling algorithms such as that presented by Cortez, Completo & Alves (2016).
- In addition to producing healthy and damaged models, one may wish to include models indicative of clinical intervention such as meniscectomy models (removal of damaged menisci to relieve the pain and restore knee joint function of OA patients). This would allow researchers to study the prolonged consequences of such treatments and their effectiveness in preventing further degradation of the joint.

- As previously mentioned, the relationship between bone and soft tissue degradation with respect to OA is yet to be fully understood. It follows, that future models should seek to investigate this link and draw conclusions about the nature of OA progression.

- The MSK approach is limited due to the simplifications of the FE model. To fully understand the knee joint behaviour, one must consider the entire MSK system response. This is due to the complex nature of loading through the leg, for example, movement of bone parts not directly located at the knee joint can cause lever arms which in turn causes change to the load going through the knee joint. This can be somewhat mitigated by analysing numerous loading scenarios on the knee joint to establish a complete understanding of its behaviour.

- Bone behaviour has been found to be time-dependent (Turner et al. 1994) and sensitive to loading frequency. The present model could be improved by incorporating this into the femur and tibia parts.

- As stated in Chapter 2, the action of mechanotransduction is yet to be fully understood and as such, future biomechanical studies may wish to update models as new anatomical data comes to light.

- To better model the trabecular bone, one may wish to use more powerful elements in FE models. The truss elements used in the current study fail to consider the rotational stiffness of the trabecular bone which will have a mechanical presence, albeit relatively small. Such improvements will come at the cost of computational expense, however, the author of this study believes that with the ever advancing progress in computational performance of FE software packages, the use of more powerful elements will become common place.

REFERENCES

Andriacchi, T. P., Mikosz, R. P., Hampton, S. J. & Galante, J. O. (1983) Model studies of the stiffness characteristics of the human knee joint. *Journal of Biomechanics.* 16 (1), 23-9.

Beaupre, G. S., Orr, T. E. & Carter, D. R. (1990) An approach for time-dependent bone modeling and remodeling - theoretical development. *Journal of Orthopaedic Research.* 8 (5), 651-661.

Bendjaballah, M. Z., Shirazi-Adl, A. & Zukor, D. J. (1995) Biomechanics of the human knee joint in compression: reconstruction, mesh generation and finite element analysis. *The Knee.* 2 (2), 69-79.

Benninghoff, A. (1925) Form und bau der gelenkknorpel in ihren beziehungen zur funktion. II. Der aufbau des gelenkknorples in seinen beziehungen zer funktion. *Zeitschrift Fue Zellforschvly.* 2 783-862.

Borelli, G. (1680) De motu animalium. *Translated as on the Movement of Animals, Translated by Maquet P.(1989), Springer-Verlag, Berlin.*

Bourgery, J. B. M. (1832)
Traite complet de lanatomie de l'homme comprenant la medecine operatoire.

Boyd, J. L., Zavatsky, A. B. & Gill, H. S. (2016) Does increasing applied load lead to contact changes indicative of knee osteoarthritis? A subject-specific FEA study. *International Journal for Numerical Methods in Biomedical Engineering.* 32 (4), e02740 (13 pp.).

Boyle, C. & Kim, I. Y. (2011) Three-dimensional micro-level computational study of Wolff's law via trabecular bone remodeling in the human proximal femur using design space topology optimization. *Journal of Biomechanics.* 44 (5), 935-942.

Burr, D. B. & Gallant, M. A. (2012) Bone remodelling in osteoarthritis. *Nat. Rev. Rheumatol.* 8 665-673.

Chern, K. Y., Zhu, W. B., Kelly, M. & Mow, V. C. (1990) Anisotropic shear properties of bovine meniscus. *Transaction of Orthopeadic Research Society.* (36), 246.

Clough, R. W. (1960) The finite element method in plane stress analysis.

Coelho, P. G., Fernandes, P. R., Rodrigues, H. C., Cardoso, J. B. & Guedes, J. M. (2009) Numerical modeling of bone tissue adaptation - a hierarchical approach for bone apparent density and trabecular structure. *Journal of Biomechanics.* 42 (7), 830-7.

Cohen, B., Gardner, R. D. & Ateshian, G. A. (1993) The influence of transverse isotropy on cartilage indentation behaviour—A study of the human humeral head. *Proceedings of the Orthopaedic Research Society.* 18 185.

Cooper, C., Dennison, E., Edwards, M. & Litwie, A. (2013) Epidemiology of osteoarthritis. *Medicographia.* 35 145-151.

Donahue, T. L. H., Hull, M. L., Rashid, M. M. & Jacobs, C. R. (2002) A finite element model of the human knee joint for the study of tibio-femoral contact. *Transactions of the ASME. Journal of Biomechanical Engineering.* 124 (3), 273-80.

Eyre, D. R., Weis, M. A. & Wu, J. J. (2005) Articular cartilage collagen: an irreplaceable framework? *European Cells & Materials.* 12 57-63.

Federico, S., La Rosa, G., Herzog, W. & Wu, J. Z. (2004) Effect of fluid boundary conditions on joint contact mechanics and applications to the modeling of osteoarthritic joints. *Transactions of the ASME. Journal of Biomechanical Engineering.* 126 (2), 220-5.

Frost, H. (2003) Bone's mechanostat: a 2003 update. *The Anatomical Record Part A: Discovery in Molecular, Celular, and Evolutionary Biology.* 275 (2), 1081-1101.

Geraldes, D. M. & Phillips, A. T. M. (2014) A comparative study of orthotropic and isotropic bone adaptation in the femur. *International Journal for Numerical Methods in Biomedical Engineering.* 30 (9), 873-89.

Guo, H., Maher, S. A. & Spilker, R. L. (2013) Biphasic finite element contact analysis of the knee joint using an augmented Lagrangian method. *Medical Engineering & Physics.* 35 (9), 1313-20.

Halonen, K. S., Mononen, M. E., Jurvelin, J. S., Toyras, J. & Korhonen, R. K. (2013) Importance of depth-wise distribution of collagen and proteoglycans in articular cartilage-A 3D finite element study of stresses and strains in human knee joint. *Journal of Biomechanics.* 46 (6), 1184-1192.

Hambli, R., Bettamer, A. & Allaoui, S. (2012) Finite element prediction of proximal femur fracture pattern based on orthotropic behaviour law coupled to quasi-brittle damage. *Medical Engineering & Physics.* 34 (2), 202-10.

Hascall, V. C., Luyton, F. P. & Plaas, A. H. K. (1990) Steady-state metabolism of proteoglycans in bovine articular cartilage. *Methods in Cartilage Research.* 108-112.

Hayes, W. C. & Mockros, L. F. (1971) Viscoelastic properties of human articular cartilage. *Journal of Applied Physiology.* 31 (4), 562-568.

Heinegard, D. (2009) Proteoglycans and more - from molecules to biology. *International Journal of Experimental Pathology.* 90 (6), 575-586.

Helgason, B., Perilli, E., Schileo, E., Taddei, F., Brynjolfsson, S. & Viceconti, M. (2008) Mathematical relationships between bone density and mechanical properties: A literature review. *Clinical Biomechanics.* 23 (2), 135-146.

Julkunen, P., Korhonen, R. K., Herzog, W. & Jurvelin, J. S. (2008) Uncertainties in indentation testing of articular cartilage: A fibril-reinforced poroviscoelastic study. *Medical Engineering and Physics.* 30 (4), 506-515.

Koch, J. (1917)
The laws of bone architecture. *American Journal of Anatomy.* 21 (2), 177-298.

Kowalczyk, P. (2010) Simulation of orthotropic microstructure remodelling of cancellous bone. *Journal of Biomechanics.* 43 (3), 563-9.

Lai, W. M., Mow, V. C. & Roth, V. (1981) Effects of nonlinear strain-dependent permeability and rate of compression on the stress behavior of articular cartilage. *Journal of Biomechanical Engineering.* 103 (2), 61-66.

Lories, R. J. & Luyten, F. P. (2011) The bone-cartilage unit in osteoarthritis. *Nature Reviews: Rheumatology.* 7 43-44-49.

Maquet, P. (1992)
Iatrophysics to biomechanics. *Journal of Bone and Joint Surgery.* 74 (3), 335-339.

Maroudas, A., Bullough, P., Swanson, S. A. V. & Freeman, M. A. R. (1968)
The permeability of Articular cartilage. *The Bone & Joint Journal.* 50-B (1), 168-173.

Mathers, C. D. & Loncar, D. (2006)
Projections of global mortality and burden of disease from 2002 to 2030. *PLoS Med.* 3 (11), 442.

Mente, P. L. & Lewis, J. L. (1994) Elastic modulus of calcified cartilage is an order of magnitude less than that of subchondral bone. *Journal of Orthopaedic Research.* 12 (5), 637-647.

Mononen, M. E., Julkunen, P., Toyras, J., Jurvelin, J. S., Kiviranta, I. & Korhonen, R. K. (2011) Alterations in structure and properties of collagen network of osteoarthritic and repaired cartilage modify knee joint stresses. *Biomechanics and Modeling in Mechanobiology.* 10 (3), 357-369.

Mononen, M. E., Mikkola, M. T., Julkunen, P., Ojala, R., Nieminen, M. T., Jurvelin, J. S. & Korhonen, R. K. (2012) Effect of superficial collagen patterns and fibrillation of femoral articular cartilage on knee joint mechanics-A 3D finite element analysis. *Journal of Biomechanics.* 45 (3), 579-587.

Mootanah, R., Imhauser, C. W., Reisse, F., Carpanen, D., Walker, R. W., Koff, M. F., Lenhoff, M. W., Rozbruch, S. R., Fragomen, A. T., Dewan, Z., Kirane, Y. M., Cheah, K., Dowell, J. K. & Hillstrom, H. J. (2014) Development and validation of a computational model of the knee joint for the evaluation of surgical treatments for osteoarthritis. *Computer Methods in Biomechanics and Biomedical Engineering.* 17 (13), 1502-1517.

Mow, V. C. & Guo, X. E. (2002) Mechano-electrochemical properties of articular cartilage: their Inhomogeneities and Anisotrpies. *Annual Review of Biomedical Engineering.* 4 175-209.

Mow, V. C., Holmes, M. H. & Lai, W. M. (1984) Fluid transport and mechanical properties of articular cartilage: A review. *Journal of Biomechanics.* 17 (5), 377-394.

Mow, V. C., Kuei, S. C. & Armstrong, C. G. (1980) Biphasic creep and stress relaxation of articular cartilage in compression: theory and experiments. *Transactions of the ASME. Journal of Biomechanical Engineering.* 102 (1), 73-84.

Phillips, A. T. M., Villette, C. C. & Modenese, L. (2015) Femoral bone mesoscale structural architecture prediction using musculoskeletal and finite element modelling. *International Biomechanics.* 2 (1), 43-61.

Phillips, A. T. M. (2012) Structural optimisation: Biomechanics of the femur. *Proceedings of the Institution of Civil Engineers: Engineering and Computational Mechanics.* 165 (2), 147-154.

Prendergast, P. J., Van Driel, W. D. & Kuiper, J. -. (1996) A comparison of finite element codes for the solution of biphasic poroelastic problems. *Proceedings of the Institution of Mechanical Engineers, Part H (Journal of Engineering in Medicine).* 210 131-5.

Reznikov, N., Shahar, R. & Weiner, S. (2014) Bone hierarchical structure in three dimensions. *Acta Biomaterialia.* 10 (9), 3815-26.

Roesler, H. (1987) The history of some fundamental concepts in bone biomechanics. *Journal of Biomechanics.* 20 (11-12), 1025-34.

Rucci, N. (2008) Molecular biology of bone remodelling. *Clinical Cases in Mineral and Bone Metabolism.* 5 (1), 49.

Rybicki, E., Simonen, F. & Weis, E. (1972) On the mathematical analysis of stress in the human femur. *Journal of Biomechanics.* 5 (2), 203-205.

Saarakkala, S., Julkunen, P., Kiviranta, P., Makitalo, J., Jurvelin, J. S. & Korhonen, R. K. (2010) Depth-wise progression of osteoarthritis in human articular cartilage: investigation of composition, structure and biomechanics. *Osteoarthritis and Cartilage.* 18 73-81.

Schinagl, R. M., Gurskis, D., Chen, A. C. & Sah, R. L. (1997) Depth-dependent confined compression modulus of full-thickness bovine articular cartilage. *Journal of Orthopaedic Research.* 15 (4), 499-506.

Toridis, T. G. (1969) Stress analysis of the femur. *Journal of Biomechanics.* 2 (2), 163-174.

Turner, C. H., Rho, J., Takano, Y., Tsui, T. Y. & Pharr, G. M. (1999) The elastic properties of trabecular and cortical bone tissues are similar: results from two microscopic measurement techniques. *Journal of Biomechanics.* 32 (4), 437-41.

van Lenthe, G., Stauber, M. & Muller, R. (2006) Specimen-specific beam models for fast and accurate prediction of human trabecular bone mechanical properties. *Bone.* 39 (6), 1182-1189.

Verhulp, E., van Rietbergen, B. & Huiskes, R. (2006) Comparison of micro-level and continuum-level voxel models of the proximal femur. *Journal of Biomechanics.* 39 (16), 2951-2957.

Voo, L., Armand, M. & Kleinberger, M. (2004) Stress fracture risk analysis of the human femur based on computational biomechanics. *Johns Hopkins APL Technical Digest (Applied Physics Laboratory).* 25 (3), 223-230.

Wilson, W., Van Donkelaar, C. C., Van Rietbergen, B., Ito, K. & Huiskes, R. (2004) Stresses in the local collagen network of articular cartilage: A poroviscoelastic fibril-reinforced finite element study. *Journal of Biomechanics.* 37 (3), 357-366.

Wilson, W., Van Rietbergen, B., Van Donkelaar, C. C. & Huiskes, R. (2003) Pathways of load-induced cartilage damage causing cartilage degeneration in the knee after meniscectomy. *Journal of Biomechanics.* 36 (6), 845-851.

Woolf, A. D. & Pfleger, B. (2003) Burden of major musculoskeletal conditions. *Bulletin of the World Health Organization.* 81 (9), .

APPENDIX

A.1 MATLAB R2016a Script used to Generate Mesoscale Bone Parts

```
% setting up a for loop so this can extended to any number of part meshes
function [ ] = createstructuralmesh(k1,meshnames)
% setting filenames

datafile01=(['nodeinfo',char(meshnames(k1)),'.txt']);
datafile02=(['SurfaceElementsMeshEL5',char(meshnames(k1)),'.txt']);
tet_elem=dlmread('tet_elem.txt',',');

% load in the nodes file
s1.nodes = dlmread(datafile01,',');
s1.numNodes = size(s1.nodes,1);


% node shift to take node numbers from 1 to ...
nodeshift=min(s1.nodes(:,1))-1;

% adjusting node numbers
s1.nodes(:,1) = s1.nodes(:,1)-nodeshift;

% load in the surface elements file
s1.triElements = dlmread(datafile02,',');

% element shift to take tri elements numbers from 1 to ...
elemshift=min(s1.triElements(:,1))-1;

% adjusting element and node numbers
s1.triElements(:,1) = s1.triElements(:,1)-elemshift;
s1.triElements(:,2) = s1.triElements(:,2)-nodeshift;
s1.triElements(:,3) = s1.triElements(:,3)-nodeshift;
s1.triElements(:,4) = s1.triElements(:,4)-nodeshift;

% for each node find the nearest nodes
% avoiding other surface nodes of the surface nodes

s1.allNodes = s1.nodes(:,1)';
s1.externalNodes = unique([s1.triElements(:,2)' s1.triElements(:,3)' s1.triElements(:,4)']);
s1.internalNodes = setdiff(s1.allNodes,s1.externalNodes);
s1.numInternalNodes = size(s1.internalNodes,2);

% set the number of connections for each node
s1.connectivity = 16;

s1.nodeConnectivity = zeros(s1.connectivity,s1.numNodes);


for n=1:s1.numNodes
  if n/100 == round(n/100)
    disp(n);
  end
  %
  clear elemlength sortelemlength
  elemlength=zeros(1,s1.numInternalNodes);
  %
```

```
    elemlength(1,:) = sqrt((s1.nodes(s1.internalNodes,2)-s1.nodes(n,2)).^2 + ...
       (s1.nodes(s1.internalNodes,3)-s1.nodes(n,3)).^2 + ...
       (s1.nodes(s1.internalNodes,4)-s1.nodes(n,4)).^2);
    sortelemlength = sort(elemlength);
    sortelemlength(1)=[];
    %
    for m=1:s1.connectivity
       s1.nodeConnectivity(m,n)=s1.internalNodes(find(elemlength==sortelemlength(m),1,'first'));
       s1.elemlengths(m,n)=sortelemlength(m);
    end
    %
End


% sorting out the element definitions
s1.elemNodes = zeros(s1.connectivity.*s1.numNodes,2);
s1.elemNodes(:,1) = (reshape(repmat((1:s1.numNodes),s1.connectivity,1),1,[]))';
s1.elemNodes(:,2) = (reshape(s1.nodeConnectivity,1,[]))';
s1.elemNodesSort = sortrows(sort(s1.elemNodes,2));
s1.elemNodesUnique = unique(s1.elemNodesSort,'rows');


%%%% start writing the Abaqus input file

s1.numCortElem = size(s1.triElements,1);
s1.numTrabElem = size(s1.elemNodesUnique,1);


% adding the the Abaqus input file
file1=fopen('mesoscale_femur_and_tibia.inp','a');
fprintf(file1,'*PART, name=Structural%s\n**\n',char(meshnames(k1)));
fprintf(file1,'*NODE\n');
for n=1:s1.numNodes
   fprintf(file1,'%i, %1.9e, %1.9e,
%1.9e\n',s1.nodes(n,1),s1.nodes(n,2),s1.nodes(n,3),s1.nodes(n,4));
end
fprintf(file1,'**\n** CORTICAL SHELL ELEMENTS\n**\n');
fprintf(file1,'*ELEMENT, TYPE=S3, ELSET=ES_CORTICAL_%s\n',char(meshnames(k1)));
for n=1:s1.numCortElem;
   fprintf(file1,'%i, %i, %i,
%i\n',s1.triElements(n,1),s1.triElements(n,2),s1.triElements(n,3),s1.triElements(n,4));
end
fprintf(file1,'**\n** TRABECULAR BAR ELEMENTS\n**\n');
fprintf(file1,'*ELEMENT, TYPE=T3D2, ELSET=ES_TRABECULAR_%s\n',char(meshnames(k1)));
for n=1:s1.numTrabElem;
   fprintf(file1,'%i, %i,
%i\n',n+s1.numCortElem,s1.elemNodesUnique(n,1),s1.elemNodesUnique(n,2));
end
for n=1:size(tet_elem,1)
   fprintf(file1,'%d, %d, %d, %d,
%d\n',n+s1.numCortElem+s1.numTrabElem,tet_elem(n,2),tet_elem(n,3),tet_elem(n,4),tet_elem(n,5
));
end
fclose('all');


%%%% finish writing the Abaqus input file



% write out the original trabecular elements
datafile03=(['trabecularelements',char(meshnames(k1)),'.txt']);
file2=fopen(datafile03,'w');
for n=1:s1.numTrabElem;
```

```
    fprintf(file2,'%i, %i,
%i\n',n+s1.numCortElem,s1.elemNodesUnique(n,1),s1.elemNodesUnique(n,2));
end
fclose('all');
```

A.2 MATLAB R2016a Script used to Adapt Mesoscale Bone Parts for Structural Efficiency

```
clear all
close all

% will always start with itnum=1
% and write this to file
itnum=1;
itnumfile=fopen('iteration.txt','w');
fprintf(itnumfile,'%i',itnum);
fclose(itnumfile);
disp(['Iteration Number ',num2str(itnum,'%04i')]);

% remove previous strain data files
% remove *.lck files
% remove abaqus reply files
dos('del strains*bars*.*');
dos('del *.lck');
dos('del abaqus.rpy.*');

stop=0;
trabecularstop=0;
corticalstop=0;

% getting the original trabecular element definitions
s1.originalElements = dlmread('trabecularelements.txt',',');
s1.nodes = dlmread('NodesSolidMeshEL5.txt',',');
s1.nodeCoords = s1.nodes(:,2:end);
s1.nodes(:,2:end)=[];

s1.originalElementNums = s1.originalElements(:,1);
s1.originalElementNodes = s1.originalElements(:,2:3);
s1.originalElementLengths = sqrt(sum((s1.nodeCoords(s1.originalElementNodes(:,2),:)-
s1.nodeCoords(s1.originalElementNodes(:,1),:)).^2,2));
s1.numElements = size(s1.originalElements,1);
s1.numNodes = size(s1.nodes,1);

% getting the original cortical element definitions
s1.originalCorticalElements = dlmread('SurfaceElementsMeshEL5.txt',',');
% finding face area for each of the cortical elements
s1.originalCorticalNodes = s1.originalCorticalElements(:,2:end);
% side vectors
s1.faceside01 = [s1.nodeCoords(s1.originalCorticalNodes(:,2),:)-
s1.nodeCoords(s1.originalCorticalNodes(:,1),:)];
s1.faceside02 = [s1.nodeCoords(s1.originalCorticalNodes(:,1),:)-
s1.nodeCoords(s1.originalCorticalNodes(:,3),:)];
s1.facecross = cross(s1.faceside01,s1.faceside02);
s1.facesize = 0.5.*sqrt(sum((s1.facecross.^2),2));
```

```matlab
while itnum<100 && stop==0


    if itnum==1
        % using a dos command to run the input file
        abaquscommand01=['abaqus job=CorticalAndTrabecularIteration',num2str(itnum,'%04i'),' int
ask_delete=OFF cpus=2'];
        disp(['  Number of Trabecular Elements: ', num2str(s1.numElements)]);
        disp('  Running the Input file...');
        [~,~]=dos(abaquscommand01,'-echo');


        % using a dos command to extract the strain data
        abaquscommand02=['abaqus cae noGUI=trabeculariterations.py'];
        disp('  Extracting information from the Output Database...');
        [~,~]=dos(abaquscommand02);
    End

    % load in the trabecular strain information
    strainfile = ['strains_trab_bars_iteration',num2str(itnum,'%04i'),'.txt'];
    s1.elementStrains = dlmread(strainfile,',');
    s1.elementNums = s1.elementStrains(:,1);
    s1.elementRefs = s1.elementNums-min(s1.originalElementNums)+1;

    % load in the cortical strain information
    % can be cleverer with what to do with this in the future...
    cortstrainfile01 = ['strains_cortSP1_bars_iteration',num2str(itnum,'%04i'),'.txt'];
    cortstrainfile02 = ['strains_cortSP2_bars_iteration',num2str(itnum,'%04i'),'.txt'];
    s1.elementcortStrains01 = dlmread(cortstrainfile01,',');
    s1.elementcortStrains02 = dlmread(cortstrainfile02,',');
    s1.elementCorticalNums = s1.elementcortStrains01(:,1);
    s1.numCorticalElements=size(s1.elementcortStrains01,1);
    s1.corticalStrain = max(abs([s1.elementcortStrains01(:,2:3)
s1.elementcortStrains02(:,2:3)]),[],2);
    %
    s1.corticalStrainTC = zeros(s1.numCorticalElements,1);
    for n=1:s1.numCorticalElements
        if s1.corticalStrain(n) == max([s1.elementcortStrains01(n,2:3)
s1.elementcortStrains02(n,2:3)]);
            s1.corticalStrainTC(n) = s1.corticalStrain(n);
        elseif s1.corticalStrain(n)*-1 == min([s1.elementcortStrains01(n,2:3)
s1.elementcortStrains02(n,2:3)]);
            s1.corticalStrainTC(n) = s1.corticalStrain(n)*-1;
        end
    end

    % finding the nodes assocaited with the existing trabecular elements
    % can be used when elements are removed
    s1.elementNodes = zeros(size(s1.elementRefs,1),2);
    for n=1:size(s1.elementRefs,1)
        s1.elementNodes(n,1:2) = s1.originalElements(s1.elementRefs(n),2:3);
    end

    % setting up a reference set of absolute strains
    % zero values for elements that have been deleted
    s1.axialStrain = zeros(s1.numElements,1);
    for n=1:size(s1.elementNums,1);
        clear a1; a1=find(s1.originalElementNums==s1.elementNums(n));
```

```matlab
    s1.axialStrain(a1)=abs(s1.elementStrains(n,2));
    s1.axialStrainTC(a1)=s1.elementStrains(n,2);
end


disp('   Performing Matlab calculations...');


% load in the previous input file
oldinputfile = ['CorticalAndTrabecularIteration',num2str(itnum,'%04i'),'.inp'];
inputfile=fopen(oldinputfile);


%read into one long string
A=fscanf(inputfile,'%c',inf);
fclose(inputfile);


% Convert into cell array, where rows=lines
B=strread(A,'%s','delimiter','\n');


%store first set of invariable lines
location1=find(strcmp(B,'**** Start of trabecular elements')==true);
C1=B(1:location1+2);


%store second set of invariable lines
location2=find(strcmp(B,'**** End of section data')==true);
C2=B(location2-1:size(B,1));


% setting it up so that the trabecular and cortical elements are arranged into different sections
if itnum==1;
    s1.previousRadii = 0.1.*ones(s1.numElements,1);
    s1.previousThickness = 0.1*ones(s1.numCorticalElements,1);
else
    location3=find(strcmp(B,'**** Trabecular Cross-Sectional Radii')==true);
    C3=B{location3+1};
    s1.previousRadii = (str2num(C3(1,6:end)))';
    location4=find(strcmp(B,'**** Cortical Thicknesses')==true);
    C4=B{location4+1};
    s1.previousThickness = (str2num(C4(1,6:end)))';
end


s1.previousArea = pi.*s1.previousRadii.^2;


target = 1250e-6;
range = 250e-6;
% increase dead zone over a number of increments
deadzone = min([250e-6 250e-6*itnum/5]);


numtrabsections = 256;
numcortsections = 256;

bonedensity=1600/(1000^3); % kg/m^3 to kg/mm^3
```

```
%%%% start of trabecular elements


nearzeroRadius=1e-3;
nearzeroArea=pi*nearzeroRadius^2;


% setting an upper limit
maxradius = 2.0;
% setting a lower limit
minradius = 0.1;


s1.sectionRadius = [linspace(minradius, maxradius, numtrabsections-1)];
%
s1.sectionArea = pi.*s1.sectionRadius.^2;


s1.newArea=zeros(1,s1.numElements);
for n=1:s1.numElements
   if (s1.axialStrain(n) > (target+range) || s1.axialStrain(n) < (target-range)) ...
      && s1.previousRadii(s1.elementRefs(n)) > nearzeroRadius
      s1.newArea(n) = s1.previousArea(n).*s1.axialStrain(n)./target;
   % allowing near zero high strain elements to 'regrow'
   elseif s1.axialStrain(n) > deadzone*(minradius/nearzeroRadius)^2 &&
s1.previousRadii(s1.elementRefs(n)) == nearzeroRadius
      s1.newArea = s1.sectionArea(1);
   else
      s1.newArea(n) = s1.previousArea(n);
   end
end


% total volume of trabecular bone
trabecularVolume = sum(s1.originalElementLengths.*s1.newArea');


% works when elements are not being eliminated
s1.elementNonZeroAreaNodes=zeros(s1.numElements,2);
for n=1:s1.numElements
   if s1.previousRadii(n) > nearzeroRadius
      s1.elementNonZeroAreaNodes(n,1:2) = s1.originalElementNodes(n,1:2);
   end
end
s1.elementNonZeroAreaNodes(s1.elementNonZeroAreaNodes==0) = [];


% deriving a connectivity matrix for the nodes
s1.nodeConnectivity=zeros(s1.numNodes,1);
for n=1:s1.numNodes
   s1.nodeConnectivity(n)=sum(sum(s1.elementNonZeroAreaNodes==s1.nodes(n)));
end
s1.nodeConnectivitymean = mean(s1.nodeConnectivity(s1.nodeConnectivity~=0));
s1.nodeConnectivitystdev = std(s1.nodeConnectivity(s1.nodeConnectivity~=0));
s1.nodeConnectivitymin = min(s1.nodeConnectivity(s1.nodeConnectivity~=0));
s1.nodeConnectivitymax = max(s1.nodeConnectivity(s1.nodeConnectivity~=0));
```

```matlab
    % finding the nearest section area value
    s1.trabecularSection=zeros(1,s1.numElements);
    for n=1:size(s1.elementNums,1);
       [~,s1.trabecularSection(s1.elementRefs(n))]=min(abs(s1.sectionArea-
s1.newArea(s1.elementRefs(n))));
       % getting rid of low radius, low strain elements
       if s1.trabecularSection(s1.elementRefs(n))==1 && s1.axialStrain(s1.elementRefs(n))<deadzone
%          && s1.nodeConnectivity(s1.originalElementNodes(s1.elementRefs(n),1)) > 4 ...
%          && s1.nodeConnectivity(s1.originalElementNodes(s1.elementRefs(n),2)) > 4
%
s1.nodeConnectivity(s1.originalElementNodes(s1.elementRefs(n),1))=s1.nodeConnectivity(s1.origi
nalElementNodes(s1.elementRefs(n),1))-1;
%
s1.nodeConnectivity(s1.originalElementNodes(s1.elementRefs(n),2))=s1.nodeConnectivity(s1.origi
nalElementNodes(s1.elementRefs(n),2))-1;
         s1.trabecularSection(s1.elementRefs(n))=0;
       end
       % this if statement could be removed to allow elements to 'regrow'
       if s1.newArea(s1.elementRefs(n))==nearzeroArea
         s1.trabecularSection(s1.elementRefs(n))=0;
       end
    end


    s1.trabecularSection=s1.trabecularSection+1;


    s1.sectionArea = [nearzeroArea s1.sectionArea];
    s1.sectionRadius = [nearzeroRadius s1.sectionRadius];
    s1.newArea = s1.sectionArea(s1.trabecularSection);
    s1.newRadii = s1.sectionRadius(s1.trabecularSection);
    trabecularsimilarity = sum(abs(s1.newArea - s1.previousArea') < 1e-6)/s1.numElements;
    trabecularelementratio =
sum(s1.newRadii>nearzeroRadius)/sum(s1.previousRadii>nearzeroRadius);
    if trabecularsimilarity > 0.99 && abs(1-trabecularelementratio) < 0.001;
       trabecularstop=1;
    end


    %%%% end of trabecular elements

    %%%% start of cortical elements


    s1.newThickness=zeros(1,s1.numCorticalElements);
    % only updateing cortical thickness every second iteration
    % as cortical bone does not respond as quickly as trabecular bone
%   if itnum/2 == round(itnum/2)
      for n=1:s1.numCorticalElements
        if s1.corticalStrain(n) > (target+range) || s1.corticalStrain(n) < (target-range)
           s1.newThickness(n) = s1.previousThickness(n).*s1.corticalStrain(n)./target;
        else
           s1.newThickness(n) = s1.previousThickness(n);
        end
      end
%   else
%      s1.newThickness = s1.previousThickness;
%   end
```

```matlab
    % setting an upper limit
    upperthicknesslimit=10;
    % setting a lower limit
    lowerthicknesslimit=0.1;


    s1.sectionThickness = [linspace(lowerthicknesslimit, upperthicknesslimit, numcortsections)];



    % finding the nearest section area value
    s1.corticalSection=zeros(1,s1.numCorticalElements);
    for n=1:s1.numCorticalElements
        [~,s1.corticalSection(n)]=min(abs(s1.sectionThickness-s1.newThickness(n)));
    % unlike trabecular elements, no cortical elements are removed
    end


    s1.newThickness = s1.sectionThickness(s1.corticalSection);



    % total volume of cortical bone
    corticalVolume = sum(s1.facesize.*s1.newThickness');


    corticalsimilarity = sum(abs(s1.newThickness - s1.previousThickness') < 1e-
6)./s1.numCorticalElements;
    if corticalsimilarity >= 0.99;
        corticalstop=1;
    end


    %%%% end of cortical elements



    % write trabecular information to another file
    % as well as the Abaqus input file
    % leaving out nearzeroRadius elements (s1.trabecularSection(n)==1);
    trabinfo=['trabecularelementsiteration',num2str(itnum,'%04i'),'.txt'];
    trabfile=fopen(trabinfo,'w');
    for n=1:s1.numElements
        if s1.trabecularSection(n)~=1
            fprintf(trabfile,'%i, %i, %i, %1.9e,
%+1.9e\n',s1.originalElements(n,1),s1.originalElements(n,2),s1.originalElements(n,3),...
            s1.sectionRadius(s1.trabecularSection(n)),s1.axialStrainTC(n));
        end
    end
    fclose(trabfile);


    % write cortical information to another file
    % as well as the Abaqus input file
    cortinfo=['corticalelementsiteration',num2str(itnum,'%04i'),'.txt'];
    cortfile=fopen(cortinfo,'w');
    for n=1:s1.numCorticalElements
        fprintf(trabfile,'%i, %i, %i, %i, %1.9e,
%+1.9e\n',s1.originalCorticalElements(n,1),s1.originalCorticalElements(n,2),...
            s1.originalCorticalElements(n,3),s1.originalCorticalElements(n,4),...
            s1.sectionThickness(s1.corticalSection(n)),s1.corticalStrainTC(n));
    end
    fclose(cortfile);
```

```matlab
%    if trabecularstop == 1 && corticalstop == 1 && itnum/2 == round(itnum/2)
    if trabecularstop == 1 && corticalstop == 1
        stop=1;
    end


    % update the iteration number
    % and write to file
    itnum=itnum+1;
    itnumfile=fopen('iteration.txt','w');
    fprintf(itnumfile,'%i',itnum);
    fclose(itnumfile);


    disp(['Iteration Number ',num2str(itnum,'%04i')]);
    disp(['   Number of Trabecular Elements: ', num2str(sum(s1.newRadii>nearzeroRadius))]);
    disp(['   Node Connectivity']);
    disp(['   Mean: ', num2str(s1.nodeConnectivitymean), ' SD: ',
num2str(s1.nodeConnectivitystdev),...
      ' Min: ', num2str(s1.nodeConnectivitymin), ' Max: ', num2str(s1.nodeConnectivitymax)]);
    disp(['   Convergence']);
    disp(['   Trabecular: ', num2str(trabecularsimilarity), ' Cortical: ', num2str(corticalsimilarity)]);
    disp(['   Trabecular Element Number Ratio: ', num2str(trabecularelementratio)]);
    disp(['   Mass']);
    disp(['   Trabecular: ', num2str(trabecularVolume), 'mm^3 Cortical: ', num2str(corticalVolume),
'mm^3']);


    infomatrix = [itnum sum(s1.newRadii>nearzeroRadius) s1.nodeConnectivitymean
s1.nodeConnectivitystdev...
        s1.nodeConnectivitymin s1.nodeConnectivitymax trabecularsimilarity corticalsimilarity
trabecularelementratio...
        trabecularVolume corticalVolume {datestr(now-floor(now))} {datestr(floor(now))}];
    aa1=['A', num2str(itnum+2)];
    aa2=['M', num2str(itnum+2)];
    aa3=[aa1,':',aa2];
    xlswrite('iterationinfo.xls',infomatrix,aa3);


    %%%%
    %%%% Writing the NEW Abaqus input file
    %%%%


    newinputfile=['CorticalAndTrabecularIteration',num2str(itnum,'%04i'),'.inp'];
    outputfile=fopen(newinputfile,'w');


    % Print first set of invariable lines
    for i=1:1:size(C1,1)
        fprintf(outputfile,'%s\n',C1{i,1});
    end


    % writing trabecular element data out to the Abaqus input file
    for n=1:s1.numElements
        %if s1.trabecularSection(n)~=0
            fprintf(outputfile,'%i, %i,
%i\n',s1.originalElements(n,1),s1.originalElements(n,2),s1.originalElements(n,3));
        %end
    end
```

```
% writing the bit between element and section definitions
fprintf(outputfile,'****\n**** End of trabecular elements\n****\n');
fprintf(outputfile,'****\n**** Start of section data\n****\n');


% writing section data out to the Abaqus input file
fprintf(outputfile,'*Elset, elset=ES_CORTICAL, generate\n');
fprintf(outputfile,'1, 10410, 1\n');
% fprintf(outputfile,'*Shell Section, elset=ES_CORTICAL, material=BONE\n');
% fprintf(outputfile,'1., 5\n');
fprintf(outputfile,'*Elset, elset=ES_TRABECULAR, generate\n');
fprintf(outputfile,'10411,229127,1\n');


% defining the cortical element sets
for n=1:numcortsections
    if sum(s1.corticalSection==n)>0;
        fprintf(outputfile,'*Elset, elset=ES_CORTICAL_%04i\n',n);
        clear a1; a1=find(s1.corticalSection==n);
        for m=1:sum(s1.corticalSection==n);
            fprintf(outputfile,'%i, ',s1.elementCorticalNums(a1(m)));
            % listed 8 elements per row
            if m/8 == round(m/8)
                fprintf(outputfile,'\n');
            end
        end
        fprintf(outputfile,'\n');
    end
end
% defining the trabecular element sets
for n=1:numtrabsections
    if sum(s1.trabecularSection==n)>0;
        fprintf(outputfile,'*Elset, elset=ES_TRABECULAR_%04i\n',n);
        clear a1; a1=find(s1.trabecularSection==n);
        for m=1:sum(s1.trabecularSection==n);
            fprintf(outputfile,'%i, ',s1.originalElementNums(a1(m)));
            % listed 8 elements per row
            if m/8 == round(m/8)
                fprintf(outputfile,'\n');
            end
        end
        fprintf(outputfile,'\n');
    end
end


% defining the cortical sections
for n=1:numcortsections
    if sum(s1.corticalSection==n)>0;
        fprintf(outputfile,'*Shell Section, elset=ES_CORTICAL_%04i, material=BONE\n',n);
        fprintf(outputfile,'%1.9e, 5 \n',s1.sectionThickness(n));
    end
end
% defining the trabecular sections
for n=1:numtrabsections
    if sum(s1.trabecularSection==n)>0;
        fprintf(outputfile,'*Solid Section, elset=ES_TRABECULAR_%04i, material=BONE\n',n);
        fprintf(outputfile,'%1.9e\n',s1.sectionArea(n));
    end
end
```

```matlab
% putting a comment in so the cortical thicknesses can be found next time round
fprintf(outputfile,'**** Cortical Thicknesses\n**** ');
fprintf(outputfile,'%1.9e, ',s1.sectionThickness(s1.corticalSection));
fprintf(outputfile,'\n');
% putting a comment in so the trabecular areas can be found next time round
fprintf(outputfile,'**** Trabecular Cross-Sectional Radii\n**** ');
for n=1:s1.numElements
    if s1.trabecularSection(n)~=0
        fprintf(outputfile,'%1.9e, ',s1.sectionRadius(s1.trabecularSection(n)));
    else
        fprintf(outputfile,'0.0, ');
    end
end
fprintf(outputfile,'\n');


% Print second set of invariable lines
for i=1:1:size(C2,1)
    fprintf(outputfile,'%s\n',C2{i,1});
end


fclose(outputfile);


%%%%
%%%% Finished writing the NEW Abaqus input file
%%%%


% using a dos command to run the new input file
abaquscommand01=['abaqus job=CorticalAndTrabecularIteration',num2str(itnum,'%04i'),' int
ask_delete=OFF cpus=2'];
disp('   Running the Input file...');
[~,~]=dos(abaquscommand01,'-echo');


% using a dos command to extract the strain data for the
% NEW output database
abaquscommand02=['abaqus cae noGUI=trabeculariterations.py'];
disp('   Extracting information from the Output Database...');
[~,~]=dos(abaquscommand02);


fclose('all');


end

matlabsendmail
```

A.3 The Biphasic Theory

The biphasic theory is the notion that a material, in this case the cartilage and menisci, is composed of both a solid and fluid phase (Almeida & Spilker, 1997). The biphasic continuum equations for soft tissues are as follows:

$$(v_i^s - \kappa p_{,i})_{,i} = 0$$

$$\sigma_{ij,j}^s + \sigma_{ij,j}^f = (C_{ijkl}^s \varepsilon_{kl} - p\delta_{ij})_{,j} = 0$$

$$\sigma_{ij}^s = C_{ijkl}^s \varepsilon_{kl} - \phi^s p\delta_{ij}$$

$$\sigma_{ij}^f = -\phi^f p\delta_{ij}$$

Where: the superscripts s and f relate to the solid and fluid phase, respectively; V^s is the time derivative (velocity) of the solid phase displacement, δ_i; K is the permeability; p is the pore fluid pressure; σ^s and σ^f are the solid and fluid phase stress tensors; ε is the solid phase strain tensor; C is the material property tensor of the solid phase; φ^s and φ^f are the solid and fluid volume fractions, respectively.

A.4 Von Mises Yield Criterion

VMS can be used to determine whether an isotropic-ductile material will yield under a complex loading condition. The VMS is compared to the yield stress of the given material to determine if failure has occurred. This is called the Von Mises Yield Criterion and is based off empirical observation.

$$\sigma_{VM} = \sqrt{\frac{(\sigma_{xx} - \sigma_{yy})^2 + (\sigma_{yy} - \sigma_{zz})^2 + (\sigma_{zz} - \sigma_{xx})^2 + 6(\tau_{xy}^2 + \tau_{yz}^2 + \tau_{zx}^2)}{2}} \qquad \text{(Eq. A.1)}$$
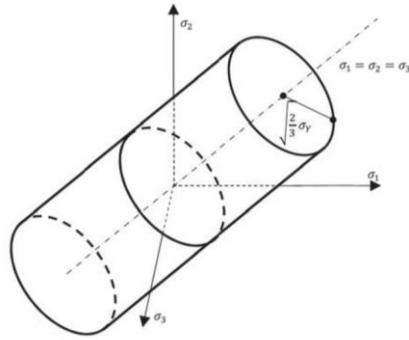

Figure A.1 3D diagram of VMS yield surface and the hydrostatic axis. (Samer Adeeb)

A diagramitic representation of the VMS yield surface in three dimensions is shown in Fig. A.1. To illustrate the stress components mentioned throughout this dissertation and their respective orientations, an image of the Cauchy Stress Tensor is shown in Fig. A.2.
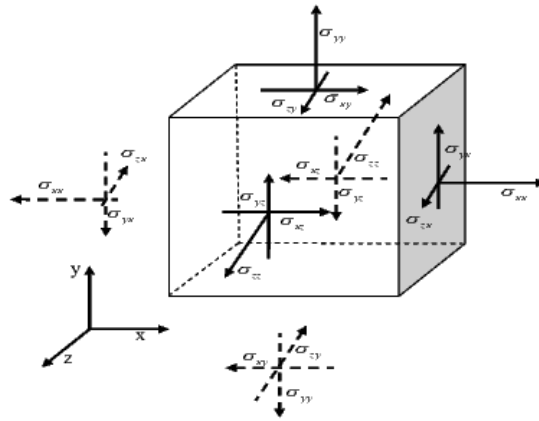
Figure A.2 Cauchy Stress Tensor. (NPTEL)

A.5 Galilei's Scaling Laws

Galilei's scaling laws are briefly touched on during the introduction of the dissertation. A more complete explanation of these laws and their relation to the field of biomechanics is given here. In the seventeenth century, it was found that the strength of tendons and bones approximately increase as a square of the linear dimensions of the tendon or bone. That is to say, for the strength of bone to double, its length must be squared. Similarly, the mass of humans and other animals follows a similar scaling law (A.3). This highlights the fact that while the size of bone changes the material itself does not and as such, large animals such as humans, are more prone to damage from bumps and falls. An intuitive example of this would be to consider a mouse and a human. If the mouse fell a distance ten times its own height, it would be unharmed, however, if a human fell a distance ten times their own height the injuries would be severe if not fatal.
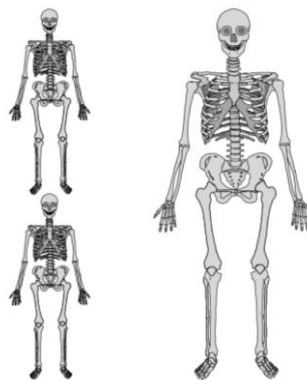

Figure A.3 Scaled human body following the strength and mass scaling law of linear dimensions squared. (University of Virginia)

A.6 Multi-point Nodal Forces on the Multiscale Knee Joint Model

As mentioned in Chapter 3, joint contact, abductor muscle, and iliotibial band forces can be applied at the head and greater trochanter of the femur to more realistically simulate the bodyweight loading condition on the femur and consequently on the knee joint.

As part of the final analysis process of the project, the nodal forces were moved down to the top face of the femur part of the present model. While this deviates from the single concentrated load application of the present study, the author wanted to investigate if the new loading condition was an improvement in terms of accuracy of results.

Figure A.4 and A.5 show the variation in VMS response across the superficial surface of the tibial cartilage and a 5 mm slice of the femur part, respectively.
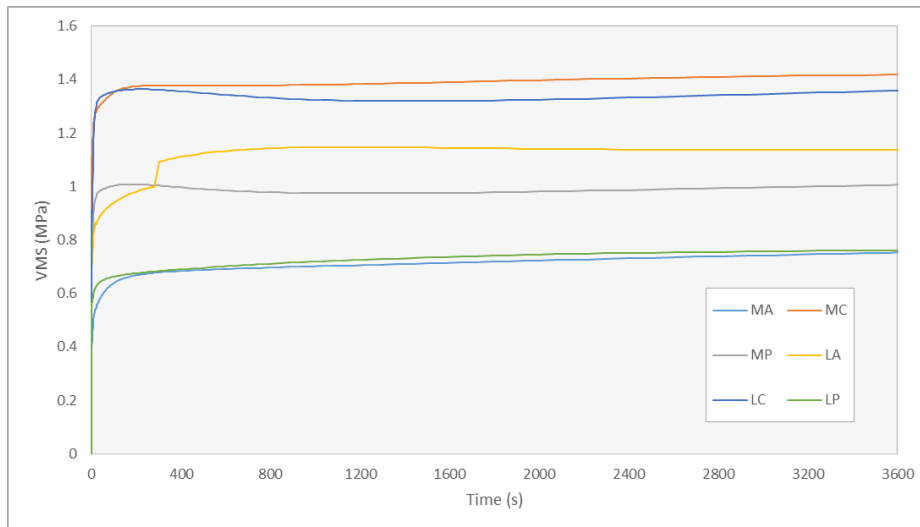

Figure A.4 VMS variation across the tibial cartilage. Note: the legend corresponds to the notations given in Chapter 4.
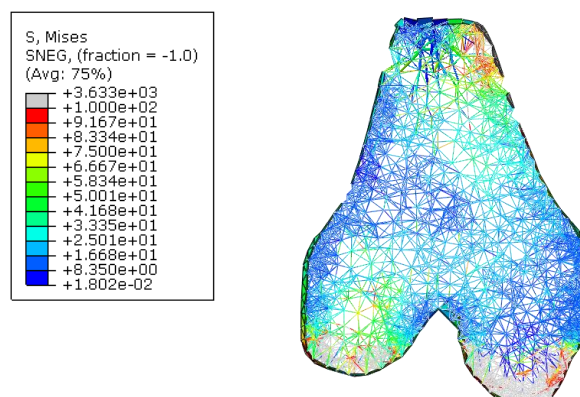
A.7 Simplified Knee Joint Model Pore Pressure Contour plots

In Chapter 3, graphs of the pore pressure response at three different soft tissue locations during one hour of bodyweight loading were presented. To better illustrate the propagation and dissipation of pore fluid throughout the simulation, contour plots of the pore pressure have been included (Fig. A.6).
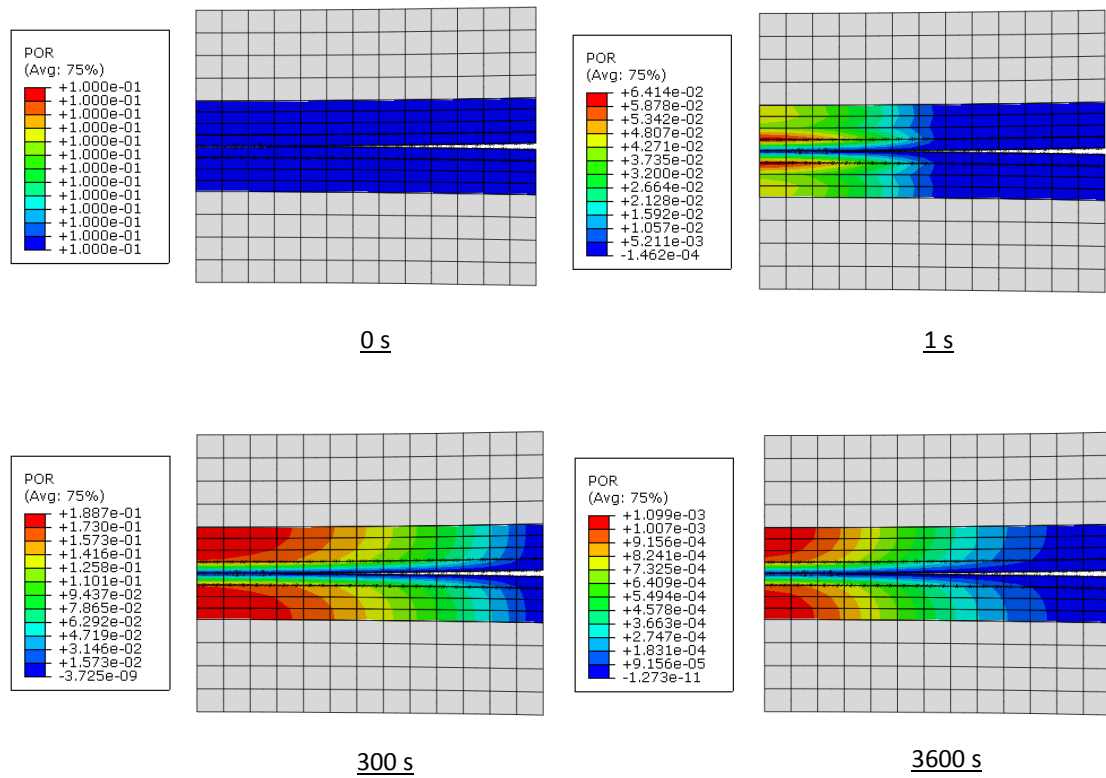

0 s

1 s

300 s

3600 s

Figure A.6 Pore pressure contour plot throughout the one-hour bodyweight loading condition.